CORROSION OF C-95, N-80, S13CR METAL AT HP/HT CONDITIONS AND THE EFFECTS OF VISCOELASTIC SURFACTANTS ON CORROSION

A Thesis

by

JUN HONG CLARENCE NG

Submitted to the Office of Graduate and Professional Studies of
Texas A&M University
in partial fulfillment of the requirements for the degree of

MASTER OF SCIENCE

Chair of Committee,	Hisham, Nasr-El-Din
Committee Members,	Berna Hascakir
	Mahmoud El-Halwagi
Head of Department,	Daniel Hill

August 2017

Major Subject: Petroleum Engineering

ABSTRACT

In the oil and gas industry, corrosion damage during treatments often occurs due to the use of corrosive treatment fluids and can result in problems such as tubular or equipment failure, and leaking. These problems can incur high costs of maintenance and pose as safety hazards to workers on site.

Hydrochloric acid (HCl) is a cheap and cost effective fluid that is commonly used in the oil and gas industry to dissolve scale and acidize formations. However, at high temperatures, it becomes extremely corrosive. Alternative acidizing fluids are typically used in place of HCl at these temperatures. However, in the event that HCl is required, corrosion inhibitors are added to the solution.

In this work, the corrosion rates of two blends of HCl based acidizing fluids were tested on C-95, N-80, and S13Cr. The results show that the corrosion rate of the acidizing fluid is the lowest for N-80 metal under all conditions tested. An increase in corrosion rates for blend A tests as acid concentration increased was observed to be higher at 280°F than at 240°F despite a 1 vol% increase in corrosion inhibitor concentration to compensate for the increase in acid concentration. The increase in corrosion rates at 240°F ranged from 0% to 9% while the range increased to 17% to 36% at 280°F. Blend B showed significant reduction in protection for N-80 at 280°F when acid concentration was raised to 20 wt% with the change in corrosion rate increasing to 68.2% from 9.2% at 240°F. In addition, VES was shown to influence the corrosion rates of N-80 and S13Cr metal negatively. The absence of VES from blend B at 280°F showed a corrosion rate of 0.0216 lb/ft^2 and 0.0159

lb/ft^2 for S13Cr and N-80, respectively. These rates increased to 0.0253 lb/ft^2 and 0.0169 lb/ft^2 with 5% VES, and to 0.0264 lb/ft^2 and 0.0187 lb/ft^2 respectively when 8% VES was used. A green coloration of the post-corrosion solution was observed when blend A was used with S13Cr metal.

DEDICATION

This work is dedicated to my parents, relatives, and friends who have supported me throughout my academic career.

ACKNOWLEDGEMENTS

I would like to thank my committee chair, Dr. Hisham Nasr-El-Din, for his unwavering support and invaluable advice throughout my research. I would also like to thank my committee members, Dr. Hascakir and Dr. El-Halwagi, for their guidance throughout the course of this research.

I would also like to express my sincere appreciation to Tariq Almubarak, who has helped me with my research projects and provided immeasurable support along the way. I also want to thank my Zhang Rixing and Tarang Lal for all their help, as well as my office mates and fellow members of my research group for the good times we've had.

Finally, thanks to my parents and brothers for their endless support and advice all these years.

CONTRIBUTORS AND FUNDING SOURCES

This work was supervised by a thesis committee consisting of Dr. Hisham Nasr-El-Din, and Dr. Berna Hascakir of the Department of Petroleum Engineering Department and Dr. Mahmoud El-Halwagi of the Department of Chemical Engineering Department.

Zhang Rixing helped carry out and monitor some of the experiments conducted. All other work conducted for the thesis was completed by the student independently.

This work was made possible in part by Well Services Group by their funding of the project.

NOMENCLATURE

HCl	Hydrochloric Acid
S13Cr	Super Chrome-13
SCC	Stress Corrosion Cracking
SSC	Sulfide Stress Cracking
LCS	Low-carbon Steel
EDTA	Ethylene diamine tetraacetic acid
NTA	Nitrilo triacetic acid
PEEK	Polyether Ether Ketone
ICP-OES	Inductive Coupled Plasma – Optical Emission Spectroscopy
VES	Viscoelastic Surfactant
NaOH	Sodium Hydroxide
SDS	Safety Data Sheet
MTR	Mill Test Report

TABLE OF CONTENTS

Page

LIST OF FIGURES

Page

LIST OF TABLES

Page

1. INTRODUCTION

1.1 Matrix acidizing

Matrix acidizing is a stimulation process where acid formulations are pumped into the formation below fracture pressure to remove damage or to enhance the flow of hydrocarbons from the formation. The goal of such treatments is to form wormholes that penetrate deep enough to bypass the damaged area or if possible, to dissolve the cause of damage. Some commonly used acids in these treatments include hydrochloric acid, hydrofluoric acid (for sandstone reservoirs), acetic acid, and formic acid. Of these acids, hydrochloric acid is the most commonly used. However, due to the use of acids, corrosion of downhole equipment is a cause for concern during acidizing treatments.

HCl is a strong mineral acid that presents many advantages when used as a stimulation fluid. These include its high dissolution strength, relatively low cost, and its ability to form soluble salts with calcium carbonate rock (Chang et al. 2008). However, this high rate of dissolution also causes it to be extremely corrosive towards metal pipes and tubulars that come into contact with it. The corrosion of these tubulars is further exacerbated as the industry drills deeper wells due to the higher temperatures at bottomhole conditions. Chloride ions from HCl are also known to facilitate pitting and crevice corrosion as they lower the pH within the confines of the pit, thereby enhancing corrosion within the pit and lowering the pitting potential of the metal (Ma 2012). Left unprotected, these metal structures will begin to leak and eventually lose their structural integrity altogether.

To understand the corrosiveness of any acidizing fluid, tests are often done using the desired formulation and metal coupons made from similar metal to the tubulars downhole. If the corrosion rate of the tested solution exceeds 0.05 lb/ft^2 for low-carbon steel or 0.02 lb/ft^2 for corrosion resistant alloys, it is too corrosive to be used (Al-Mutairi et al. 2005; Kalfayan 2008). However, this standard may be lowered in lieu of other factors such as the cost of the metal used or ease of replacement and material transportation (Gaverick 1994). Pitting of the coupon is also taken into consideration when analyzing the results of the test as pits can severely undermine the structural integrity of the metal. In the oil and gas industry alone, costs incurred due to the corrosion amount to approximately $1.372 billion dollars annually (Popoola et al. 2013).

1.2 Corrosion

Corrosion is an interaction between a material and its environment that results in the eventual destruction of the material. It can be classified into eight different types (Fontana and Greene, 1978). They are: uniform corrosion, galvanic corrosion, crevice corrosion, pitting corrosion, intergranular corrosion, selective leaching, erosion corrosion, and stress-corrosion cracking. Each corrosion type involves a different mechanism of attack and thus require different methods of prevention. The types of corrosion are elaborated below:

1.2.1 Uniform Corrosion

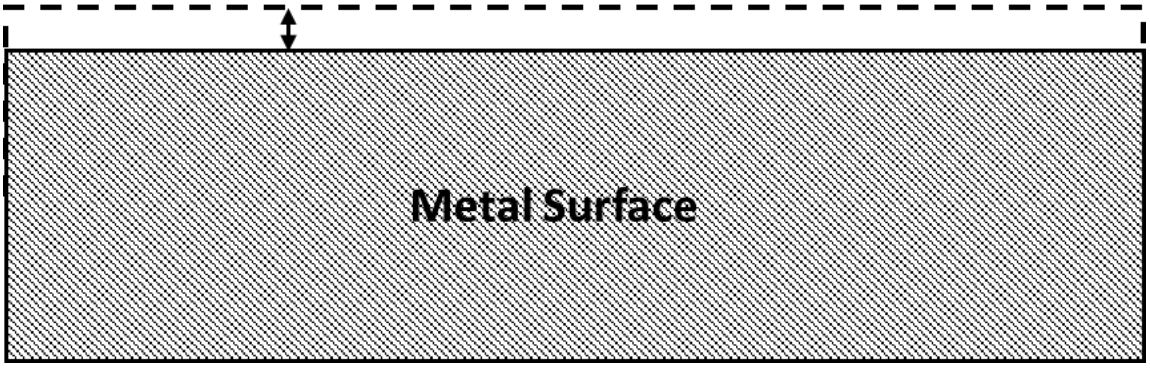

Figure 1: Uniform Corrosion of metal surface.

Uniform corrosion is an idealized type of electrochemical corrosion that involves even corrosion of the metal surface over time as shown in Figure 1. For this type of corrosion to occur, an electrochemical cell consisting of a cathode, an anode, an aqueous medium, and a metallic/electronic path is required.

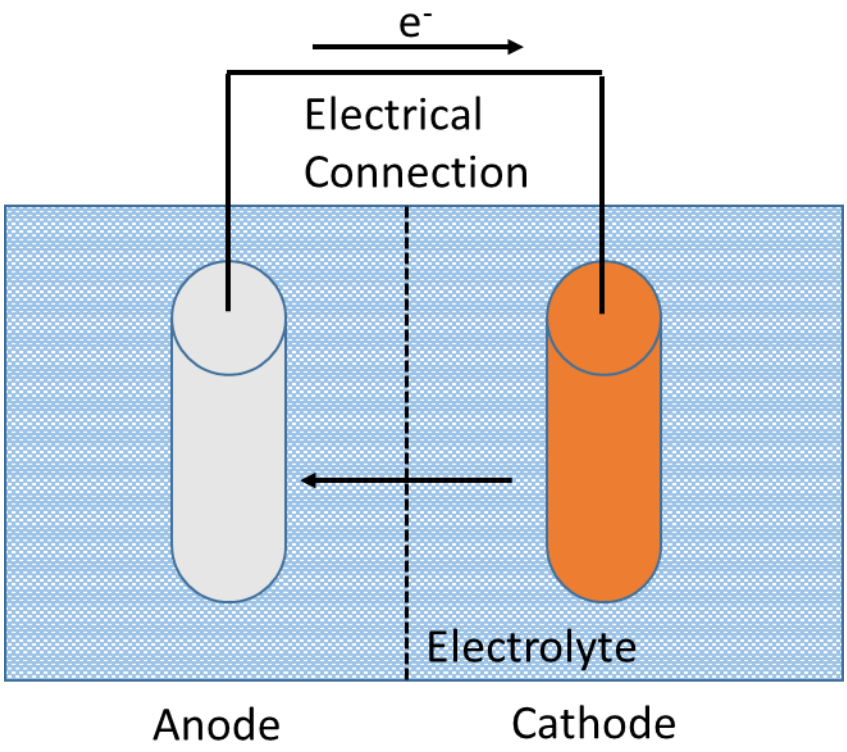

Figure 2: Example of electrochemical cell.

Due to factors such as grain structure, alloying, and temperature, a single solid piece of metal surface can possess multiple anodic and cathodic sites. Cathodic sites facilitate the evolution of hydrogen gas while anodic sites involve the dissolution of metal surface. This type of corrosion is assumed when conducting corrosion tests as it presents a simple way to compare test results and to determine the lifespan of the material. However, most corrosion problems are a combination of corrosion types and thus localized corrosion problems must also be thoroughly investigated.

1.2.2 Pitting Corrosion

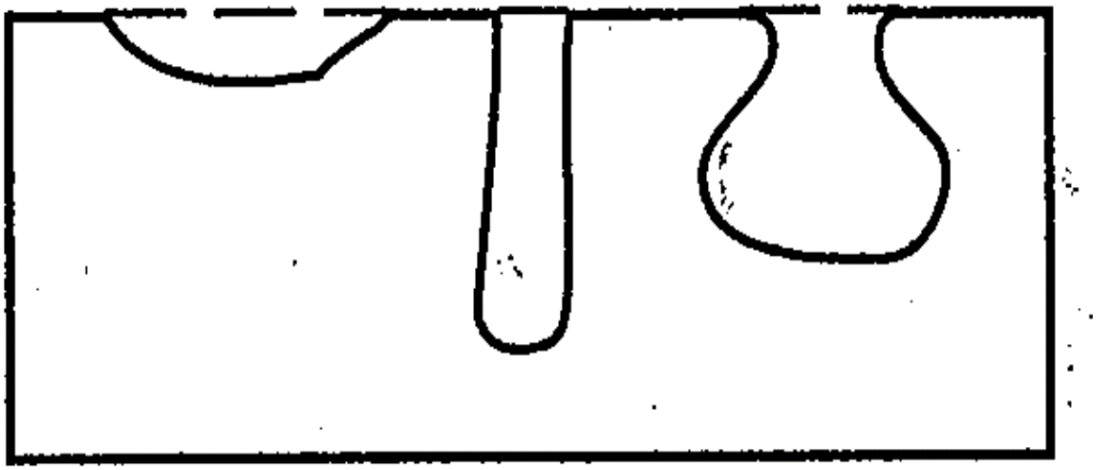

Figure 3: An example of pitting corrosion (Jones 1996)

Continuous removal of metal from the same anodic site results in pitting corrosion and appear as depressions or holes in the metal surface. Pit sizes can vary from microscopic to large visible gaps. Despite their small size, pits can severely weaken the mechanical properties of the metal and result in catastrophic failure. These pits form randomly on the metal surface and can widen beneath the metal surface as shown in Figure 3 due to highly corrosive environment formed within the pit. Furthermore, corrosion products originating from the pit can deposit at the mouth, covering up the presence of a pit. As a result, areas susceptible to pit formation are difficult to predict and a rigorous monitoring system is needed to detect and address any pitting problems occurring. The presence of certain anions such as chlorides and bromides may increase the tendency of certain types of metal to pit and must be avoided or controlled.

1.2.3 Crevice Corrosion

Crevice corrosion is similar to pitting corrosion in that it forms small defects in the metal surface that grow due to a localized corrosive environment. The difference between the two is that crevice corrosion occurs in small gaps between structures which tend to be relatively sheltered from flow of the bulk layer. These gaps exist due to design and facilitate the creation of a highly corrosive environment. Both crevice and pitting corrosion are enhanced in the presence of certain anions which serve to lower the pitting potential of the metal. Due to this, crevice corrosion can be more easily addressed since the locations favoring this type of corrosion are known.

1.2.4 Galvanic Corrosion

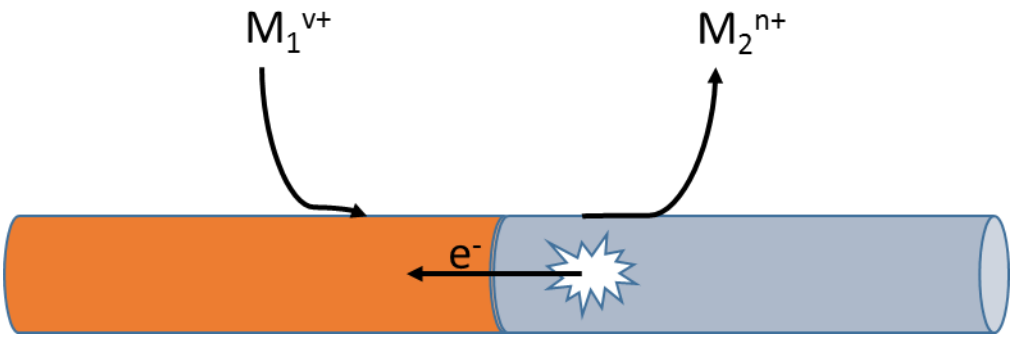

Figure 4: Galvanic corrosion in two dissimilar metals.

This type of corrosion is an electrochemical corrosion that occurs due to the coupling of two dissimilar metals in a corrosive environment as shown in Figure 4. The more anodic material will experience a localized attack near the boundary of the joint

resulting in damage to the pipe wall. This can occur in the oil and gas industry in surface pipelines transporting seawater or other corrosive solutions.

1.2.5 Selective Leaching

The presence of a corrosive solution can result in selective leaching in metal alloys where more anodic components are removed more readily from the alloy than others (e.g. zinc leached preferably instead of copper when using brass). This leaching leaves behind a porous copper structure with poor mechanical properties (Jones 1996) that would eventually result in mechanical failure of the material.

1.2.6 Intergranular Corrosion

Intergranular corrosion occurs in alloys due to segregation of impurities, depletion of passivating elements at areas adjacent to grain boundaries (forming depleted zones), or the precipitation of carbides at the grain boundary (Jones 1996). This results in the depleted zone being more susceptible to corrosion. The formation of cathodic carbides can also result in localized galvanic corrosion. The formation of depleted zones is also known as sensitization and commonly occurs in stainless steels after being exposed to high temperatures. Such corrosion also results in increased vulnerability of the alloy to stress cracking.

1.2.7 Stress Corrosion Cracking and Hydrogen Embrittlement

Stress corrosion cracking (SCC) and hydrogen embrittlement occur due to excessive stress placed on localized spots on the metal originating from localized corrosion such as pitting or intergranular corrosion. These forms of corrosion generally originate in pits where stress can accumulate at the tip of the pit. In acidic environments, hydrogen atoms formed on the surface through electrochemical corrosion can diffuse into the lattice where it can recombine within the metal to form localized pockets of H_2 gas. As the volume of gas increases, increased stress is exerted on the metal structure that can eventually cause the stressed area to crack and rupture. In sour environments, sulfide deposits accelerate this process as they act as H_2 poisons and hinder the recombination of hydrogen atoms.

1.2.8 Erosion Corrosion

Erosion corrosion occurs due fast flowing corrosive fluid impacting the surface of the metal. Such a fluid would be able to corrode through other forms of corrosion but due to its high speed, it would also be able to physically remove the layer of corrosion products deposited on the metal surface. Removal of these products exposes fresh metal to the corrosive solution thereby accelerating corrosion (Jones 1996).

1.3 Corrosion in the Oil and Gas Industry

In the oil and gas industry, the use of strong acids and presence of chloride ions results in uniform corrosion, crevice corrosion, and pitting corrosion as the most prevalent

forms of corrosion (Finsgar 2014). Under specific conditions, such as in the presence of hydrogen sulfide, other forms of corrosion, such as sulfide stress cracking, can also occur. Corrosion by strong acids such as HCl on metals can be primarily described by an electrochemical process. Initially, the acid dissolves the oxide layer of the metal, be it Fe(III) or Cr(III) oxide depending on the type of metal dissolved. This reaction is a typical acid-base reaction and proceeds according to the following equations:

Fe(III) oxide:

$Fe_2O_3 + 6HCl \rightarrow 2FeCl_3 + 3H_2O$. ……..…….…….(1)

Cr(III) oxide:

$CrO_3 + 3HCl \rightarrow CrCl_3 + 1.5H_2O$. ……..……(2)

The oxide layer on the surface of the metal is generated by oxidation of the base metal in air. This layer protects the bulk of the metal from exposure to the environment and its thickness is principally dependent on temperature and the time the metal is exposed to air, with increased exposure and higher temperatures resulting in thicker oxide layers (Humpston and Jacobson, 2004).

After dissolving this layer, the electrochemical reaction between the bulk metal and H^+ ions in the solution occurs. Due to imperfections in the metal, local cathodic and anodic sites develop on the metal surface that facilitate corrosion. At the cathodic sites, using mild steel as an example, reduction of H^+ ions occurs through the donation of a pair of electrons from Fe atoms at the anodic site. Such a reaction follows Eqs. 3 and 4:

Cathodic:

$2H^+ + 2e^- \rightarrow H_2$. ……..……..……(3)

Anodic:

$Fe(s) \rightarrow Fe^{2+} + 2e^-$. ……(4)

The overall electrochemical reaction can be expressed in Eq. 5:

$2H^+ + Fe(s) \rightarrow H_2 + Fe^{2+}$. ……...……(5)

Certain compounds present in the metallic structure can affect the corrosion rate of the metal. One such example is cementite. Cementite is a form of iron carbide that has been shown to accelerate corrosion by providing a favorable cathodic site with lower overpotential for the formation of hydrogen (Ferhat et al., 2014).

1.4 Alloys in the Oil and Gas Industry

In the oil and gas industry, metals of construction can be divided into two distinct categories: low carbon steels (LCS) and corrosion resistant alloys (CRAs). LCS such as N-80, H-40 or J-55 grade steels are often used to cast tubulars, casings or pipes that are used downhole or to transport fluids around the facility. CRAs such as 13Cr, S13Cr, and 316L, and nickel-based CRAs such as Hastelloy, Incoloy, and Alloy C-276, are commonly used in environments too corrosive for LCS and are some of the more widely used CRAs in the oil and gas industry (Craig and Smith 2011). A summary of the properties and the compositions of some of these metals can be found in Table 1.

Table 1: Material composition and yield strength of some API grade metals commonly used in the oil and gas industry (API Spec 5CT 2005).

Metal	Composition (wt%)								Yield Strength (ksi)
	C	Mn	Cr	Ni	Cu	S	P	Si	
H-40	-	-	-	-	-	<.03	<.03	-	40.0-80.0
J-55	-	-	-	-	-	<.03	<.03	-	55.0-80.0
L-80	<.43	<1.9	-	<.25	<.35	<.03	<.03	<.45	80.0-95.0
13Cr	.12-.22	.25-1.0	12.0-14.0	<.5	<.25	<.02	<.01	<1.0	80.0-95.0

As implied by their name, carbon steels are a mix between carbon and steel, with the prefix 'low' or 'high' referring to the percentage composition range of carbon contained in the mixture. Low carbon steels contain less than 0.4%, medium carbon steels contain 0.4% to 0.6%, and high carbon steels contain 0.6% to 1.5% carbon. LCS are the preferred choice of material when downhole conditions are determined to be less corrosive. This is due to their low cost relative to other steels such as chrome steel, ease of manufacture, and their ability to withstand the physical stresses of downhole conditions. In the event that higher yield strength is required, LCS alloys such as P-110 can be used.

As the search for more sources of oil widens, formations containing corrosive gases such as H_2S, CO_2 or a combination of both need to be tapped. Both H_2S and CO_2 form acidic solutions when dissolved in aqueous media while H_2S presents the additional problem of Sulfide Stress Cracking (SSC). In order to control corrosion from these gases, casings and tubulars made of CRAs are often used in place of LCS. Due to the broad definition of the word corrosion, it must be understood that CRAs are not impervious to all forms corrosion. Instead, they are metals that display high levels of corrosion resistance

specifically in the environment they are in without requiring either inhibition or mitigation techniques (Petersen and Bluem 1989). CRAs typically form a layer of Cr_2O_3 in air which confers superior resistance to CO_2 corrosion. However, concentrated HCl can dissolve this layer, resulting in severe corrosion to the base metal (Al-Mutairi et al. 2005).

SSC is a cathodic cracking mechanism that occurs in metals in the presence of aqueous H_2S and is a form of hydrogen embrittlement. This will eventually result in mechanical failure of the metal structure, and is a problem common to certain grades of CRAs (Zhao et al. 2003). SSC is also accelerated by the presence of FeS formed by H_2S reacting with the metal surface since FeS is a hydrogen poison. Due to these many considerations, selecting the appropriate metallurgy can be difficult balance between cracking resistance, corrosion resistance, and costs (Kane and Cayard 1998).

1.5 Effects of Alloying

Alloying is the process of adding other elements to a base metal in order to enhance its existing physical and chemical properties or to give it new ones. This depends on the element added and the extent of it depends on the quantity of element alloyed. Alloying involves both metallic elements, such as chromium, and non-metallic elements, such as carbon. It is important to know the composition of the metal in question as it can provide insight to the occurrence and extent of corrosion in the wellbore.

Some elements commonly added to steel include:

- Carbon (C) is one of the main components of steel. It is added in order to form carbides and martensite that add hardness to the steel. Wear resistance of steel also

increases with higher carbon content. However, excessive carbon results in increased brittleness and reduced toughness of the steel. The content of carbon in steel is indicated through the terms ‘low’, ‘medium’, and ‘high’ as described earlier. In the presence of H_2S, low carbon content can also help mitigate SSC (Ueda et al. 1996). The composition of carbon can also affect electrochemical corrosion. The higher the quantity of carbon, the less ferritic and more pearlitic phases present. Since the presence of pearlite reduces anodic corrosion, a higher carbon content can reduce corrosion of carbon steels. However, too much carbon will convert the pearlite into cementite which accelerates corrosion (Tourky et al. 1965).

- Manganese (Mn) is often added with the intention of removing sulfur impurities and oxides through the precipitation of MnS and by reducing oxides. It also allows the formation of finer divided microstructures in steel, giving rise to increased strength and reducing the ductile transition temperature (Cunat 2004). It also increases the rate and stability when cooling steel while reducing the shock experienced by the structure during quenching. Mn is also cheaper than other alloying elements such as nickel and have thus been used as nickel substitutes.
- Nickel (Ni) in steel acts in a similar fashion to Mn, though it is also more expensive than Mn. It improves the hardness of steel by causing finer microstructures and the rate of cooling of steel but in a more drastic and irregular manner. High Ni content in steel increases its hardness, strength, and oxidative resistance at the cost of

ductility (Cunat 2004). The carbon content of the steel is also known to influence the behavior of alloyed Ni.

- Chromium (Cr) is often alloyed with steel to grant corrosion and oxidation resistance to the metal. This occurs through the formation of a thin layer of Cr oxide on the surface of the metal, (Cunat 2004). Steels with approximately 11% Cr are known as stainless steels. Alloying Cr to steel also improves wear resistance and hardness.
- Molybdenum (Mo) is well-known for its ability to prevent and repassivate localized corrosion sites through action of its molybdate anion (Kodama and Ambrose 1976). It is also added to increase the hardness, tensile strength at high temperatures, and mechanical strength of steel. It is seldom used alone and commonly used along with other elements such as Cr or Ni.
- Vanadium (V) increases the toughness and strength of steel by inhibiting grain growth during heat treatment. It can also induce secondary hardening and act as an oxygen scavenger.
- Copper (Cu) is mainly used to enhance the resistance of steels to atmospheric corrosion. At concentrations above 0.2%, it is also helps provide resistance to certain types of acids such as sulfuric acid, as well as pitting resistance (Craciunescu and Hamdy 2013).
- Silicon (Si) is found in almost every alloy of steel as it is added primarily as a deoxidizer and to provide oxidation resistance (Cunat 2004). It is also known to

increase the strength of ferrite, the toughness, and the hardness of steel (Cunat 2004).

- Phosphorous (P) is usually present as an impurity but can be deliberately added to steel in order to increase its machinability, yield strength, and corrosion resistance (Townsend, 2001). However, at concentrations greater 0.04%, phosphorous will instead result in a reduction in toughness and weldability. Therefore, the concentration of phosphorous in steel must be controlled.

1.6 Corrosion Control during Treatments

In order to avoid damage or injury resulting from corrosion during acidizing operations, steps must be implemented to hinder the corrosion process. There are several methods of corrosion control that have been used. These include:

- Replacing HCl in favor of milder acidizing fluids
- Replacing steel tubulars for ones constructed from acid-resistant metals
- Adding corrosion inhibitors and intensifiers

It must be noted that corrosion will still occur no matter which methods or combination of methods are used and cannot be completely prevented. However, by reducing corrosion rate, the cost of damages resulting from corrosion can be reduced and the safety of personnel ensured.

Due to the high cost of acid-resistant metals such as Hastelloy, using them in place of steel tubulars completely in order to resist acid corrosion is not economically feasible.

However, insertion or replacement of sections of tubulars with Hastelloy grade metal may be a viable long term solution if the environment in that particular area is deemed to be too corrosive such in high temperature sour wells containing carbon dioxide (Vaughn and Greer, 1980). In these cases, however, galvanic corrosion from contact between different steel grades can also pose a problem.

Alternative acidizing fluids such as organic acids and chelating agents can be used in place of HCl. These fluids are less corrosive than HCl and do not form sludges in crude oil with high asphaltene content (Bujise et al., 2004). Another advantage of using alternate acidizing fluids over HCl is their ability to penetrate deep into the formation. The high reaction rate of HCl causes high levels of face dissolution and thus compromises its ability to form wormholes and penetrate the rock (Crowe et al., 1988). However, these alternative fluids also present several disadvantages. The calcium salts of some organic acids, such as acetic and formic acid, have been shown to precipitate when high concentrations of acid is used (Chang et al., 2008). This limits the concentration of organic acid that can be used. They also do not react to completion and cost more than HCl per mass of rock dissolved (Chang et al., 2008). Chelating agents such as ethylene diamine tetraacetic acid (EDTA) or nitrilo triacetic acid (NTA), can present environmental and health concerns when used (Nowack, 2002). They are also expensive, and can degrade when exposed to certain high temperatures, rendering them ineffective.

Corrosion inhibitors are chemicals that are injected along with acidizing fluids in order to protect the metal structure and reduce the need for frequent replacement of tubulars due to corrosion damage. Corrosion inhibitors can either come in the form of a liquid, such as

thiourea, or that of a gas, like carbon monoxide, though liquids are more commonly used in acidizing fluids. Corrosion inhibitors can be classified into three groups based on their inhibiting mechanism: cathodic inhibitors, anodic inhibitors, and mixed inhibitors (Rostami and Nasr-El-Din, 2009). In matrix acidizing, organic inhibitors behaving as mixed inhibitors are most commonly used. These inhibitors work by adsorbing to the surface of the metal to block active metal sites, forming a thin film over the metal surface in the process. This film prevents direct interaction between the environment and the metal while blocking off both anodic and cathodic reaction sites, thus inhibiting corrosion.

The potency of corrosion inhibitors, however, suffers beyond its maximum operating temperature. To address this, corrosion inhibitor intensifiers are added to the fluid mix. Some examples of intensifiers commonly used in the oilfield include copper salts, antimony salts, potassium iodide, formamides, and formic acid (Frenier et al. 1989; Seth et al. 2011). More recently, however, antimony and copper salts are seldom used due to toxicity and environmental reasons. Intensifiers act to enhance the performance of the paired corrosion inhibitor, to increase the operating temperature range, and to increase their tolerance to other additives (Singh and Quraishi, 2015). This is especially important as deeper wells are drilled since the temperature of the formation increases with well depth.

2. MATERIALS AND EQUIPMENT

2.1 Materials

N-80, S13Cr, and C-95 coupons used in these tests were purchased from OFI Testing Equipment. The coupons measured approximately 1 in. in width, 1.5 in. in length and 1/16 in. in thickness. Two circular holes located 3/16 in. from the end of each side with a diameter of 0.15 in. were also cut at either end of the coupon. These holes are used to insert PEEK screws that allow the coupon to be attached to a circular Hastelloy impeller which doubles up as a coupon holder. The coupons were physically isolated from the surface of the impeller using PEEK washers.

Since the Mill Test Report (MTR) for the coupons was unavailable, the composition of the coupons was determined by dissolving it in 20 wt% HCl and testing the filtered and diluted solution using Inductive Coupled Plasma – Optical Emission Spectroscopy (ICP-OES) to determine the ion concentration. The concentration of the 5 major elements present in the metals were tested along with other minor elements such as sulfur, phosphorous, and silicon. Certain elements such as carbon could not be detected. The elemental composition of each metal can be found in Table 2.

Table 2: Composition of metals used as determined through ICP analysis. Certain elements such as carbon could not be determined.

Metal ions (%)	ICP Analysis		
	N-80	C-95	S13Cr
Fe	98.8	98.5	84.8
Mn	1.1	0.6	0.8
Mo	-	-	0.5
Cr	-	0.8	12.8
Ni	-	-	1
Others	0.1	0.1	0.1

All additives used throughout the test were obtained from Baker Petrolite except the iron control agent, which was obtained from BASF. 36.4 wt% HCl used to prepare the solution was obtained from Macron Fine Chemicals. NaOH and chromium (III) chloride were obtained from Sigma Aldrich.

2.2 Equipment

Corrosion tests were carried out using a model 4523 benchtop reactor manufactured by Parr Instruments Company. The reactor vessel has a capacity of 1 liter and is made of Hastelloy B-2 metal. Hastelloy is a registered trademark by Haynes International Inc. and is made predominantly from nickel. It typically contains approximately 66% Ni, 2% Fe, 1% Cr, 28% Mo, 1% Mn, and 1% Co. Its composition makes it extremely resistant to reducing acids such as HCl, pitting corrosion, and stress corrosion cracking. The vessel

has an internal diameter of 4” and a depth of 5.4”. It has a maximum pressure tolerance of 1900 psi and a maximum operating temperature of 350°C. The reactor vessel is sealed using Teflon gaskets and attached to the reactor head with C clamps made from Hastelloy B-2. The vessel is heated using a 1000 W calrod heater that is controlled using a reactor controller. A thermowell is built into the reactor and a thermocouple is used to determine the temperature in the reactor vessel.

A schematic and picture of the reactor can be found in Figure 5. The reactor head is directly connected to a rotating shaft that is powered by a 1/8 hp motor and has a maximum rpm of 1700. It also has an inlet, two outlets located on either end of the head. The inlet to the reactor has 2 feeds and a sampling valve which run through a dip tube to the base of the vessel. One of the feeds is connected to a N_2 gas tank to allow pressurized N_2 gas to pressurize the reactor vessel while the other runs from a 300 ml Teflon lined liquid charging pipette. N_2 gas is fed to the reactor and the pipette through rubber hoses.

The sampling valve is connected to a ¼” Hastelloy pipe with gate valves on each end. Samples can be taken by first opening the sampling valve while the gate valves are closed, then closing the sampling valve and opening the lower gate valve to release the fluid. One outlet of the reactor leads to a 600 ml Hastelloy B-2 scrubber system through a ¼” Teflon lined stainless steel pipe. A filtered dip tube runs to the base of the scrubber to allow for sparging so that acidic vapors generated from the reaction can be neutralized before being released. The other outlet is used to house the rupture disc. The rupture disc outlet is connected via ¼” stainless steel piping to a 1 liter plastic bottle in order to prevent spraying of hot acidic fluids in the event that the rupture disc bursts.

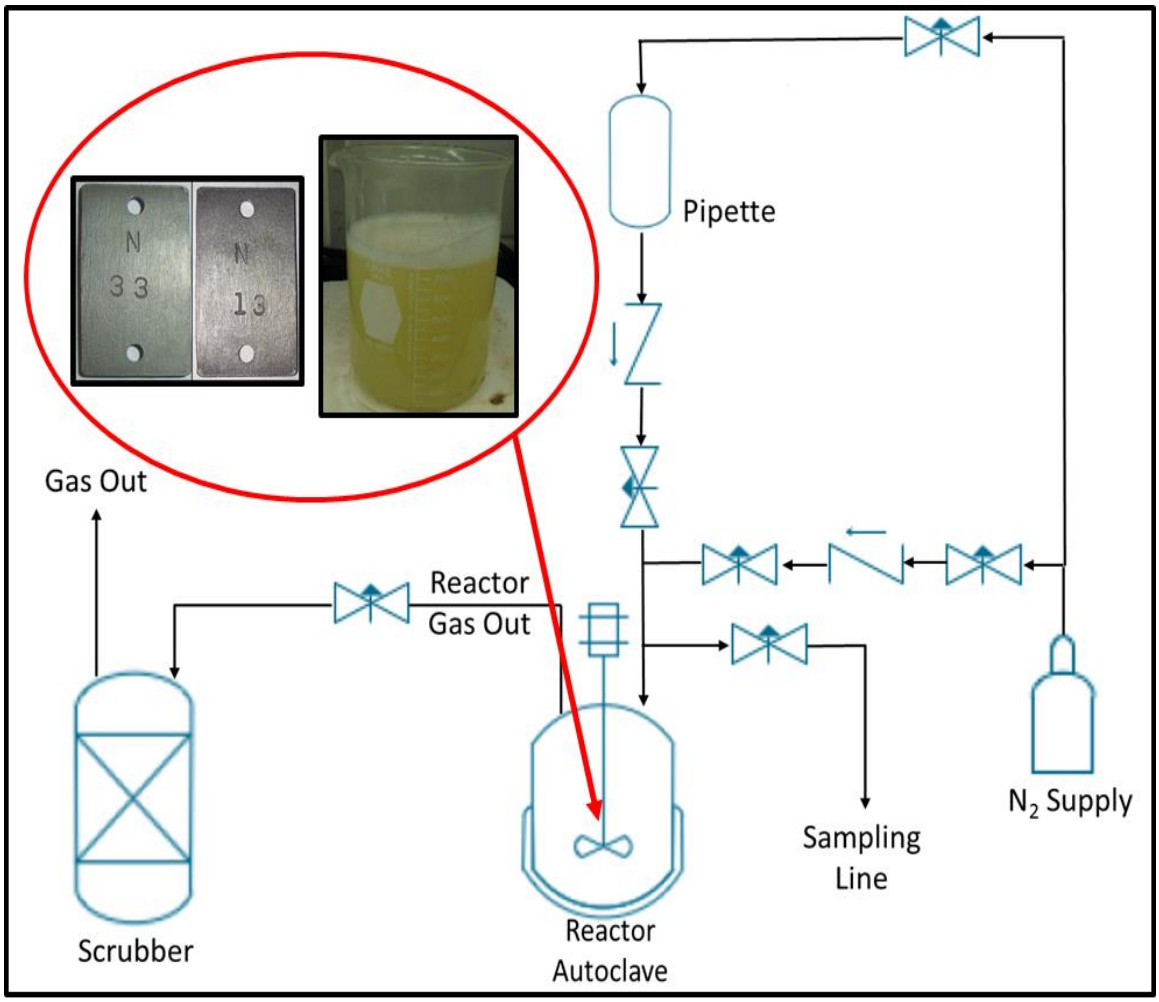

Figure 5: Schematic of autoclave used for corrosion tests.

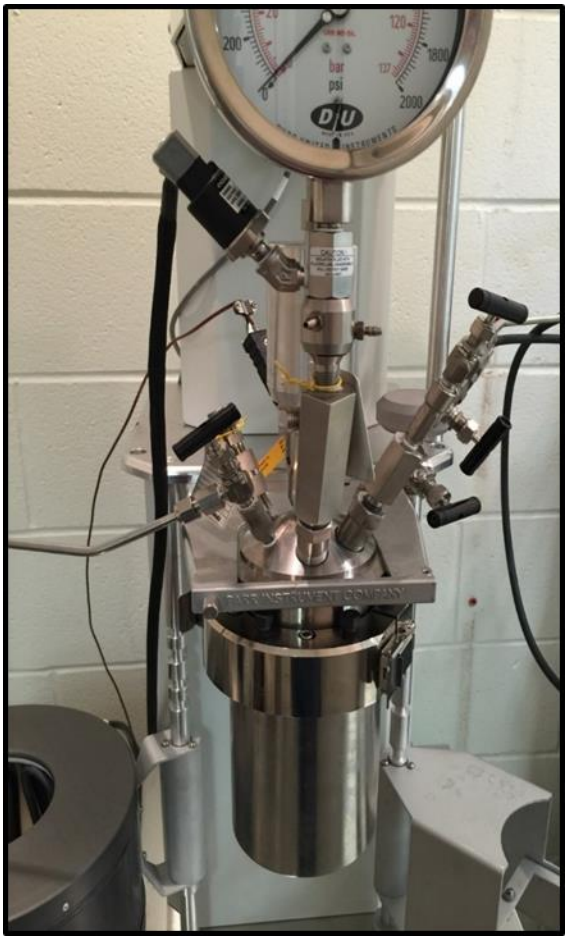

Figure 6: Picture of reactor used for corrosion testing.

Inductive Coupled Plasma – Optical Emission Spectroscopy (ICP-OES) was used to determine the concentration of Fe, Cr, Mn, Mo, and Ni in the solution after each test. ICP-OES excites vaporized metal ions using plasma generated by heated argon gas. The electromagnetic radiation resulting from the excitation is unique to each metal element and can be interpreted by the machine using pre-determined standards. 5, 15, and 30 ppm standards are made by diluting a 1000 ppm nitric acid matrix standard and run for each of the 5 ions before testing the diluted samples.

Figure 7: Optima 7000 DV Inductive Coupled Plasma - Optical Emission Spectroscopy machine by PerkinElmer.

The detection range of the ICP equipment is therefore set between 0 ppm and 30 ppm, and the post-corrosion samples are diluted so that the concentration of each ion falls within that range. After obtaining the concentrations of the diluted samples, these values were multiplied by the dilution factor to obtain the original concentration of each ion. The ICP equipment used was an Optima 7000 DV ICP-OES made by PerkinElmer.

2.3 Preparation

2.3.1 Solution Preparation

800g of acid solution was prepared for each test according to a specific formulation as shown in Table 3.

Table 3: Formulation for blends A and B (Blend A uses inhibitor A, blend B uses inhibitor B).

Temperature (°F)	240				280			
HCl (wt %)	15		20		15		20	
Inhibitor A (vol %)	2	-	3	-	2.5	-	3.5	-
Inhibitor B (vol %)	-	2.5	-	2.5	-	3	-	3
VES (vol %)	-	5	-	5	-	5	-	5
Additives (vol %)	5	7	5	7	7	7	7	7

For blend B, the VES was added slowly to the stirred solution at 200 rpm to prevent the formation of "fish eyes" in the solution. After all the VES was added, the mixture was mixed at 400 rpm for 5 minutes to ensure complete mixing of the VES. Both acid solutions were mixed with a magnetic stirrer for at least 10 minutes before being added to the vessel. Pictures of the acid solution was obtained prior to adding it to the reactor in order to observe for any color changes during the test. For the VES tests on corrosion rate, Blend B was prepared in the same manner as before using the same amount of each chemical with the exception of VES.

For the scrubber, a solution of 5 wt% NaOH was prepared by dissolving 8 g of NaOH tablets in 400 ml of DI water. The NaOH tablets were measured out using a digital weigh scale with 1 mg accuracy. This solution was used to scrub the outlet gas of HCl vapor.

Chromium (III) chloride solution for color testing was prepared by dissolving 0.17 g of $CrCl_3 \bullet 6H_2O$ salt was dissolved in 1L of DI water in order to create a 100 ppm solution. This solution was then added to the filtered and diluted samples to test for the green color.

2.3.2 Coupon Preparation

Two metal coupons were prepared for corrosion testing according to ASTM G31-12a. They were washed thoroughly with DI water and acetone before being allowed to dry off

in air. The coupons were polished using sugar blasting by the manufacturer and thus no further polishing was carried out. After the drying the coupons, a vernier caliper was used to measure the dimensions of each coupon. The weight of each coupon was obtained using a mass balance with 1 mg accuracy. Finally, pictures of the front and back of each coupon were obtained to document the state of the coupon surface before the test.

2.4 Procedure

2.4.1 Corrosion Tests

The coupons were attached to either side to the impeller using 3/8" PEEK screws while PEEK washers were used to prevent physical contact between the impeller and the coupon. This was to avoid galvanic corrosion of the coupon. The impeller was subsequently mounted on to the rotating shaft and the acid solution was added to the reactor vessel as shown in Figure 8.

Figure 8: Coupon mounted to rotating shaft of reactor.

The vessel was sealed and pressurized with N_2 gas to test for leaks. After no leaks were found, the gas outlet valve was opened without stopping the N_2 inlet flow to purge the system of O_2. Once complete, the outlet valve was closed, the inflow of N_2 stopped, and the heater switched on. Throughout the test, the system pressure was maintained above 1200 psi. At the end of 6 hours, the heater was switched off and the vessel allowed to cool. At this time, N_2 was used to purge the vapor space in the reactor of HCl vapor. After 5

minutes of purging, the reactor was allowed to depressurize. The scrubber was filled with 400 ml of dilute NaOH to neutralize the acidic vapors resulting from the test.

Once cooled, the coupons were carefully extracted from the reactor, washed with DI water, cleaned with a non-metallic brush, rinsed with acetone, and then allowed to dry. A sample of the used acid solution was taken to be filtered and diluted for ICP while the remainder was poured into a 1L Pyrex flask to observe any color changes. Pictures of the solution were taken in order to document its final color. The weight of the dried coupons was then taken and recorded in order to determine the corrosion rate in lb/ft^2. Pictures of the front and back of the corroded coupons were compared to the photos taken before corrosion to determine pitting corrosion.

For the tests for the effect of VES on corrosion rates, only N-80 and S13Cr coupons were used. 0% and 8% VES solutions were tested with 15% HCl over a duration of 6 hours at 280°F and pressure above 1200 psi. Similar to the previous corrosion tests, pictures of the coupons and the acid solutions were taken before and after testing for comparison.

2.4.2 Color Test

When blend A was used with S13Cr coupons, the end solution became green in color. ICP testing on the solutions showed that this was likely due to the presence of Cr^{3+} ions in the solution. To test this, samples from blend A and blend B corrosion tests were filtered and a dilute solution of chromium (III) chloride was added to those not containing Cr^{3+}. The color of the resulting solution was then visually compared to that from the blend A-

S13Cr test. This solution of chromium (III) chloride was prepared by dissolving a small quantity of chromium (III) chloride in DI water.

3. RESULTS

The average corrosion rates obtained are shown in Table 4 and Table 5. The corrosion rates for most of the tests were within the 0.05 lb/ft^2 industry standard for low-carbon seel with the exception of tests at 280°F with C-95 and 20 wt% HCl. At these conditions, the corrosion rate of C-95 hovered at the acceptable limit for both blends of acids. As for S13Cr, the corrosion rates at 280°F were above the acceptable limit of 0.02 lb/ft^2. Pitting corrosion of the acid solutions were not significant in any of the tests conducted.

From these results, several observations regarding the results and the chemicals used can be drawn. The first is the relatively low corrosion of N-80 than C-95 and S13Cr. The second is the effectiveness of the corrosion inhibitor in both blends A and B as the conditions of the solution are varied. Generally, as acid concentration and temperature increase, the inhibition efficiency of the corrosion inhibitor appears to decrease.

Table 4: Summary of average corrosion rates for blend A and B acid solutions for all tests.

Blend A							
240°F				280°F			
15% HCl		20% HCl		15% HCl		20% HCl	
C-95	0.0159	C-95	0.0173	C-95	0.0368	C-95	0.0503
N-80	0.0117	N-80	0.0113	N-80	0.0240	N-80	0.0281
S13Cr	0.0145	S13Cr	0.0149	S13Cr	0.0297	S13Cr	0.0389

Blend B							
240°F				280°F			
15% HCl		20% HCl		15% HCl		20% HCl	
C-95	0.0119	C-95	0.0154	C-95	0.0291	C-95	0.0461
N-80	0.00883	N-80	0.00964	N-80	0.0169	N-80	0.0284
S13Cr	0.0113	S13Cr	0.0149	S13Cr	0.0253	S13Cr	0.0409

From Table 5, an increase in VES concentration was found to result in a corresponding increase in corrosion rates of N-80 and S13Cr coupons.

Table 5: Corrosion rate for blend B solutions with different VES concentrations on S13Cr and N-80 at 280°F.

Corrosion Rate (lb/ft^2)		
VES	S13Cr	N-80
0% VES	0.0216	0.0159
5% VES	0.0253	0.0169
8% VES	0.0264	0.0187

Examples of changes in the appearance of the coupons used before and after the tests can be found in Figure 9. Examples of each blend's color before and after can be found in Figure 10 and Figure 11.

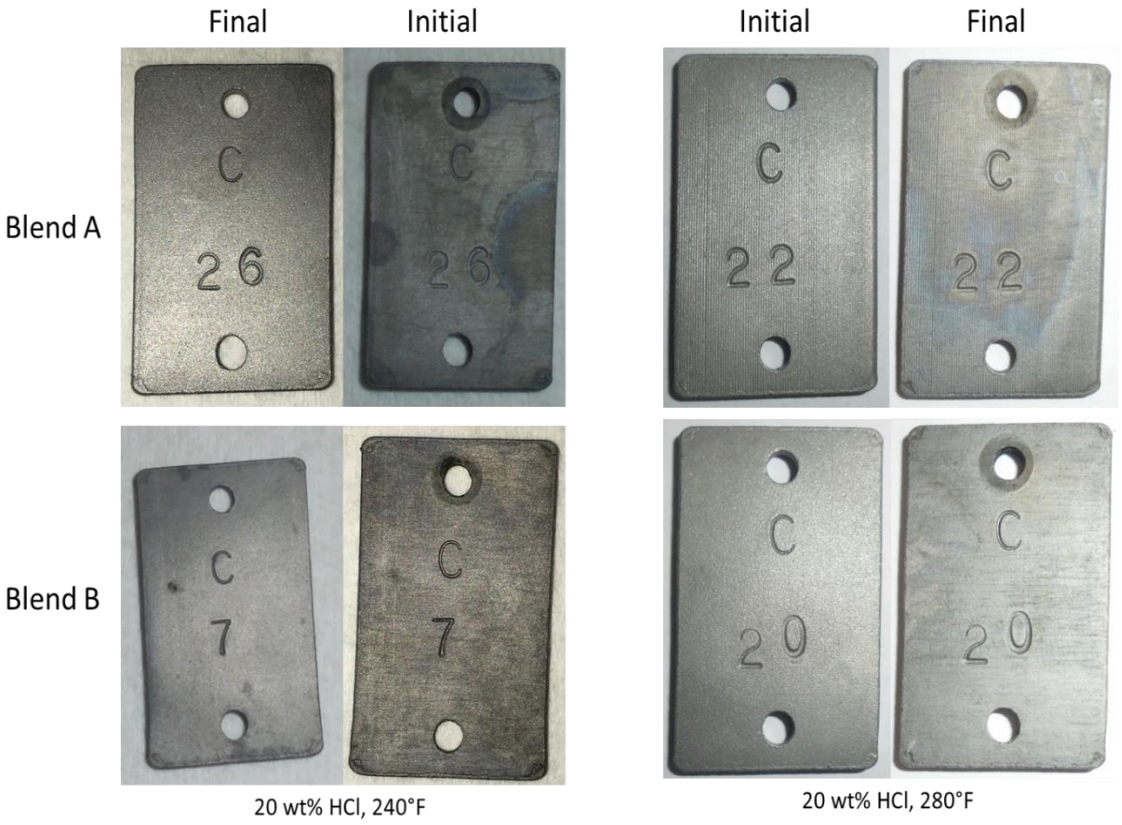

Figure 9: Examples of coupons before and after corrosion testing.

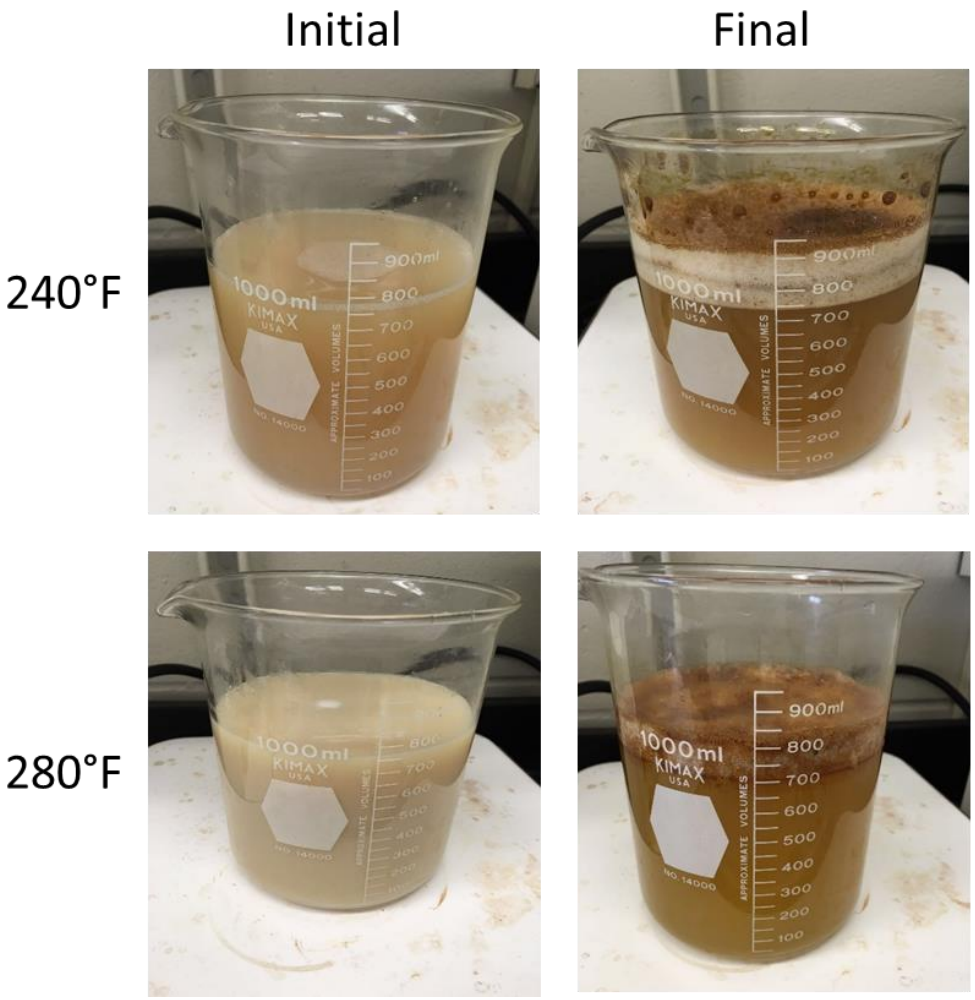

Figure 10: Examples of color change of blend A solutions before and after corrosion tests.

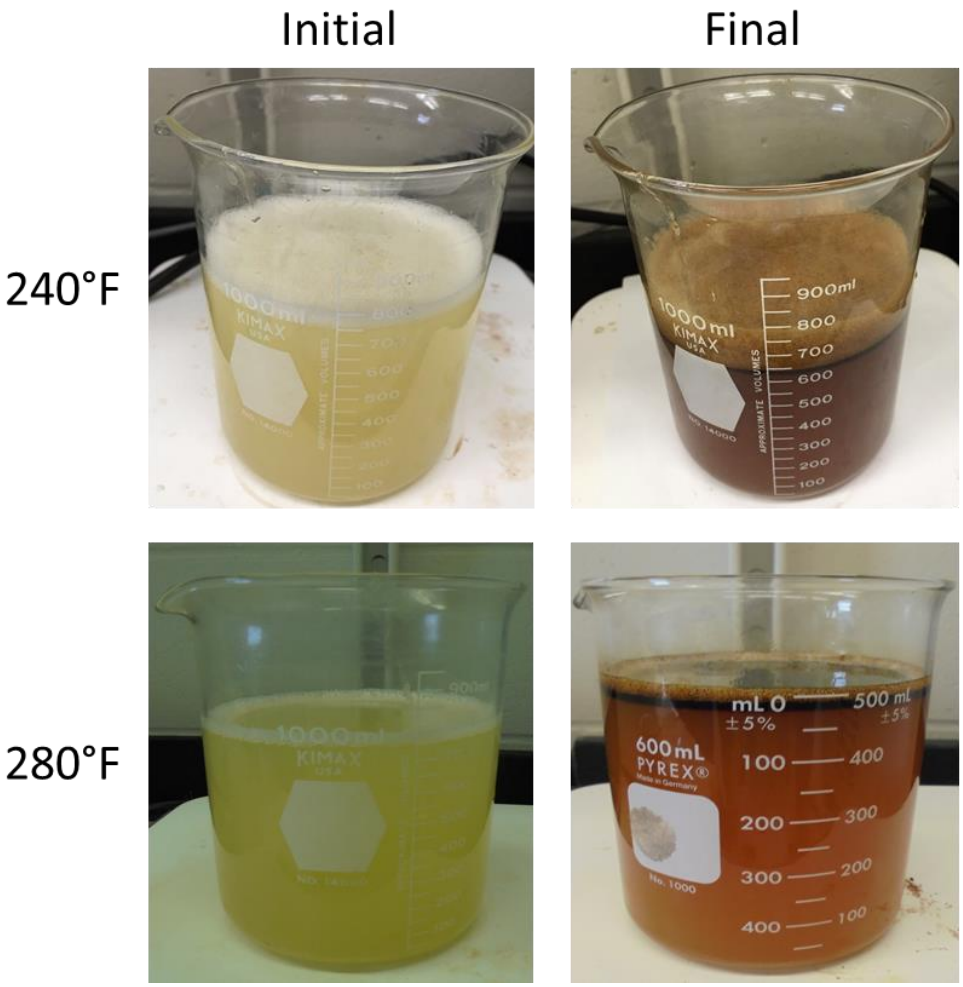

Figure 11: Examples of color change in blend B before and after testing.

4. DISCUSSION

In order to explain the results obtained, the Safety Data Sheet (SDS) of each additive was reviewed and the active ingredient identified. A literature review of the ingredients of each additive was then conducted to identify any possible impact on corrosion (inhibition or acceleration). From this, it was determined that the only additives responsible for corrosion inhibition were the corrosion inhibitor and the corrosion inhibitor intensifier. HCl was identified as the single source of corrosion.

4.1 Lower corrosion rate of N-80

Across all tests, the corrosion rate of N-80 was also found to be lower than that of S13Cr and C-95. This can be seen from Figure 12 and Figure 13 where the corrosion rates of N-80 are lower than C-95 and S13Cr for both blends at all conditions. To confirm this observation, the corrosion rate was estimated from ICP-OES results and can also be found in Figure 12 and Figure 13 for both blends of acid. This was done using the concentration of the Fe, Mn, Mo, Ni, and Cr ions obtained from ICP tests.

The corrosion rates obtained from the ICP results confirm the trend observed. However, the values calculated were found to yield a higher corrosion rates that those obtained by the weight loss method. This is because the ICP data includes ions that were corroded from the Hastelloy vessel and the other Hastelloy components immersed in the acid solution.

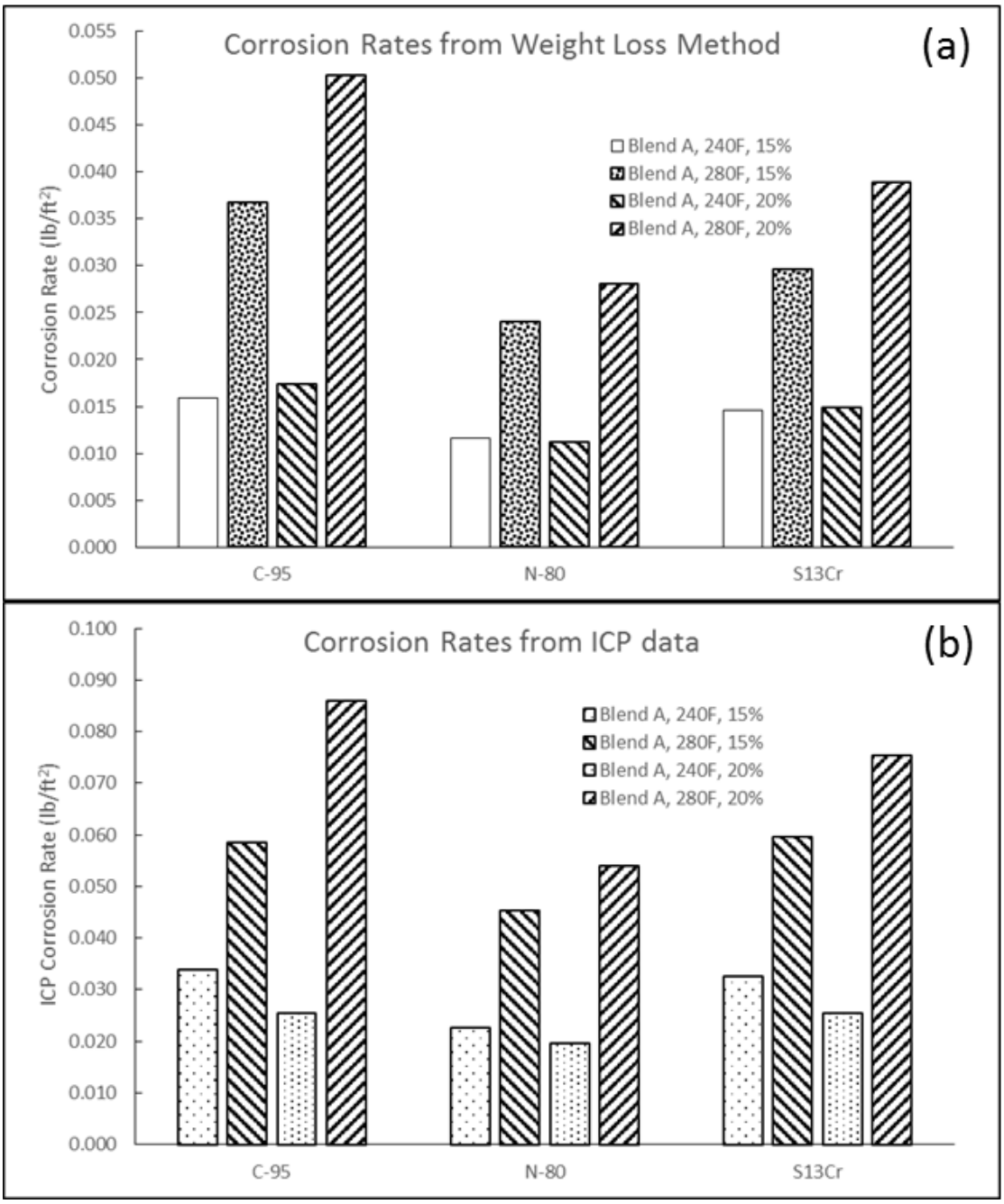

Figure 12: Corrosion rates in lb/ft^2 determined by the (a) weight loss method and by (b) ICP-OES results for blend A solution.

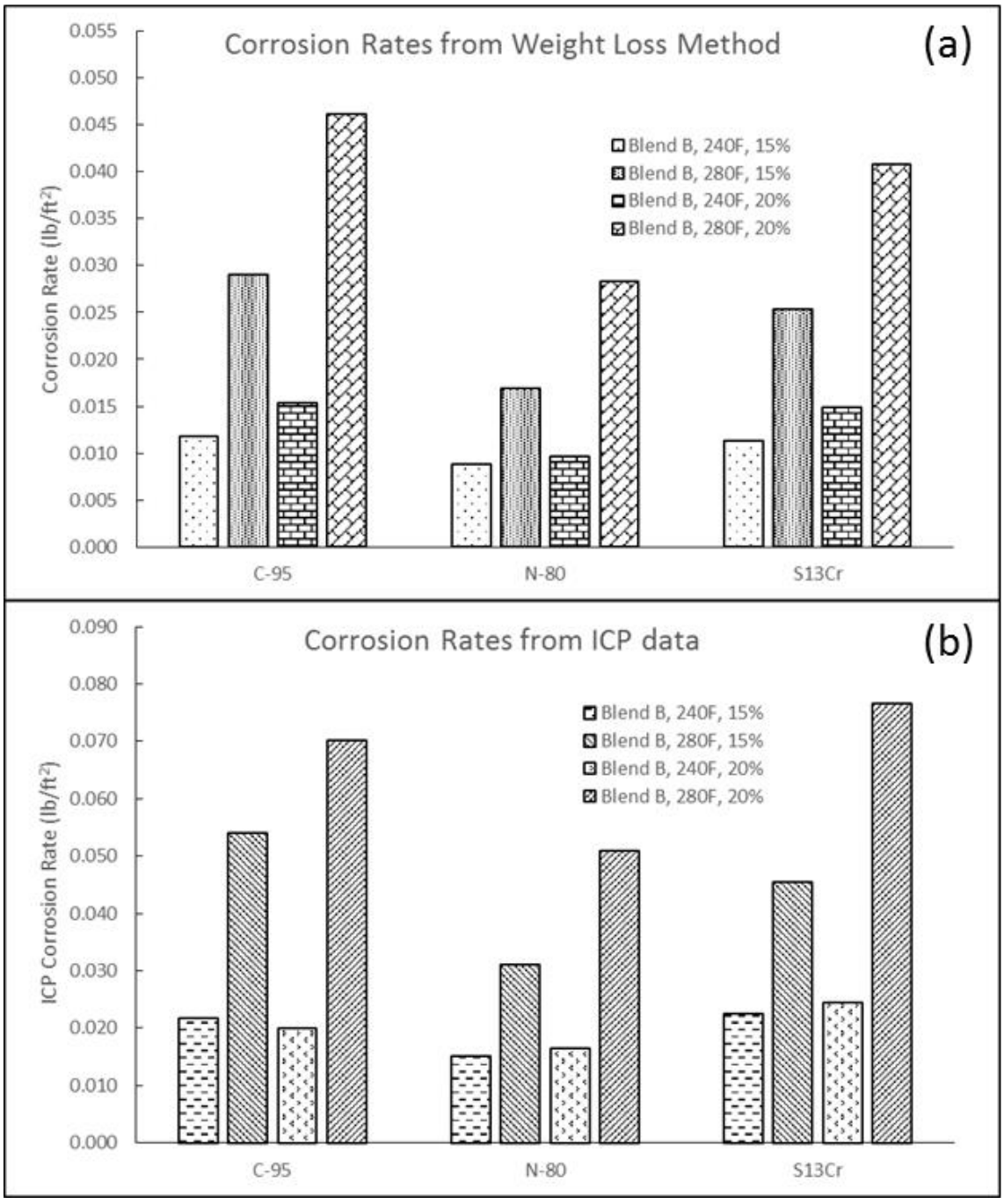

Figure 13: Corrosion rates in lb/ft^2 determined by the (a) weight loss method and by (b) ICP-OES results for blend B solution.

This result was interesting as N-80 and C-95 are both carbon steels with martensitic structures (Devereux 1998) and yet yielded greatly differing corrosion rates. A search of

literature showed that this is likely due to the presence formic acid used as the corrosion inhibitor intensifier. Formic acid is often added as a corrosion inhibitor intensifier in order to extend the working temperature range of the corrosion inhibitor. It provides inhibition to corrosion through the formation of carbon monoxide (CO) through a dehydration reaction that occurs in the presence of a strong acid, high temperatures and catalyzed by a metal surface (Cassidy et al. 2007).

Decomposition of formic acid on steel in strong acids occurs according to Eqs. 6 to 9 (Cassidy et al. 2007):

$HCOOH + HCl \leftrightarrow HCOOH_2^+ + Cl^-$. ……(6)

$HCOOH_2^+ \leftrightarrow\ HCO^+ + H_2O$. ……..(7)

$Cl^- + HCO^+ \leftrightarrow\ CO\ (soln) + HCl$. ……..……..(8)

$CO\ (soln) \rightarrow CO(gas)$. ……..…….(9)

Carbon monoxide adsorbs to the surface of the metal as shown in Figure 14. By doing so, it blocks active sites on the surface thereby preventing corrosion. Linear bonds (1 Fe atom to 1 CO molecule) are formed in low concentrations of CO gas. As more formic acid decomposes, these bonds become bridging bonds (2 or more Fe atoms to 1 CO atom) allowing a single CO molecule to inhibit corrosion on multiple sites (Cassidy et al. 2007; Raval et al. 2015).

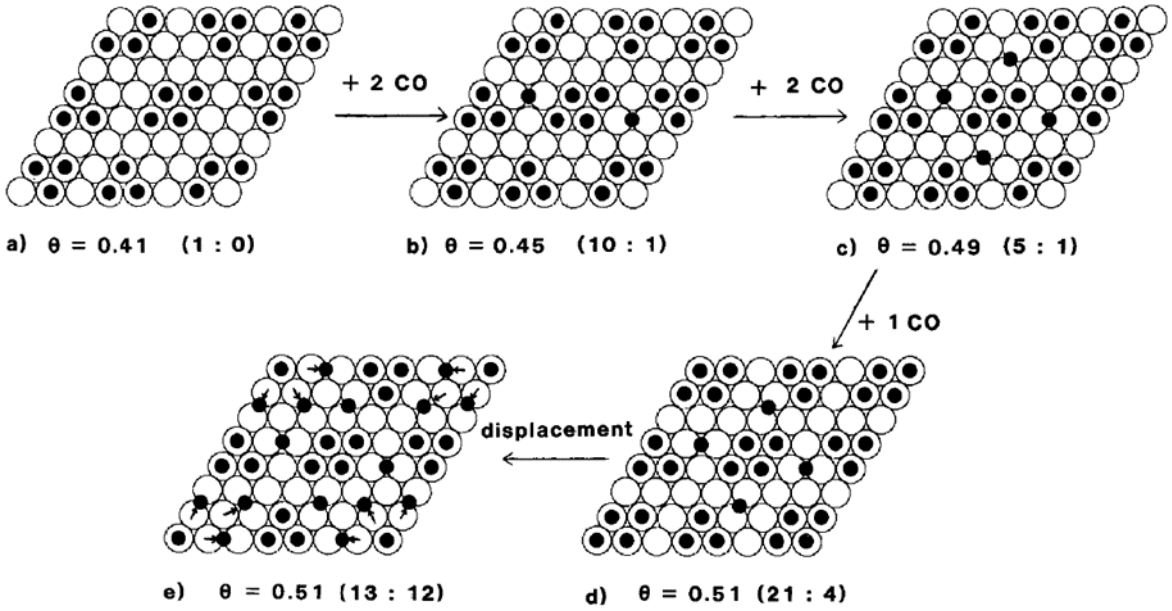

Figure 14: Adsorption of CO to Fe on surface to form linear bonds and bridging bonds depending on the amount of CO produced (Raval et al. 2015).

Similar to the observations made in Figure 12, tests carried out by Cabello et al. (2013) investigating the inhibition capabilities of formic acid and carbon monoxide show that when formic acid was used as an inhibitor with N-80 metal, a large inhibition of H_2 evolution is observed. However, the same level of inhibition was not achieved when a carbon monoxide saturated solution was used. Other metals tested, namely I825 and U420, did not exhibit low corrosion rates when exposed to formic acid inhibition as compared to N-80. As a result, another product of formic acid is thought to be formed on the surface of N-80. This product is believed to be a residue of formic acid that is not formed at room temperature and pressure and adsorbs strongly to its surface (Cabello et al., 2013). However, since C-95 and N-80 are both low-carbon steels and have similar microstructure, it is unlikely that formic acid would decompose differently on both.

Therefore, it is possible that this observation is caused by the slight difference in the composition of both steels. The secondary reaction of CO on the steel surface involves further decomposition of CO on the Fe surface which leads to the formation of a layer of metal carbides (Kehrer and Leidheiser 1954, Broden et al. 1976). While iron carbides can promote corrosion by increasing the H_2 overpotential, they can also reduce corrosion rates if their particle size is large enough (Ferhat et al. 2014). The carbon content of the steel could not be measured by ICP. Since these metals are both LCS, the initial carbon content should be similar. The difference in composition may have affected the size of the iron carbides formed and thus resulted in the difference in corrosion rates.

4.2 Reduced effectiveness of Inhibitor A at higher temperature

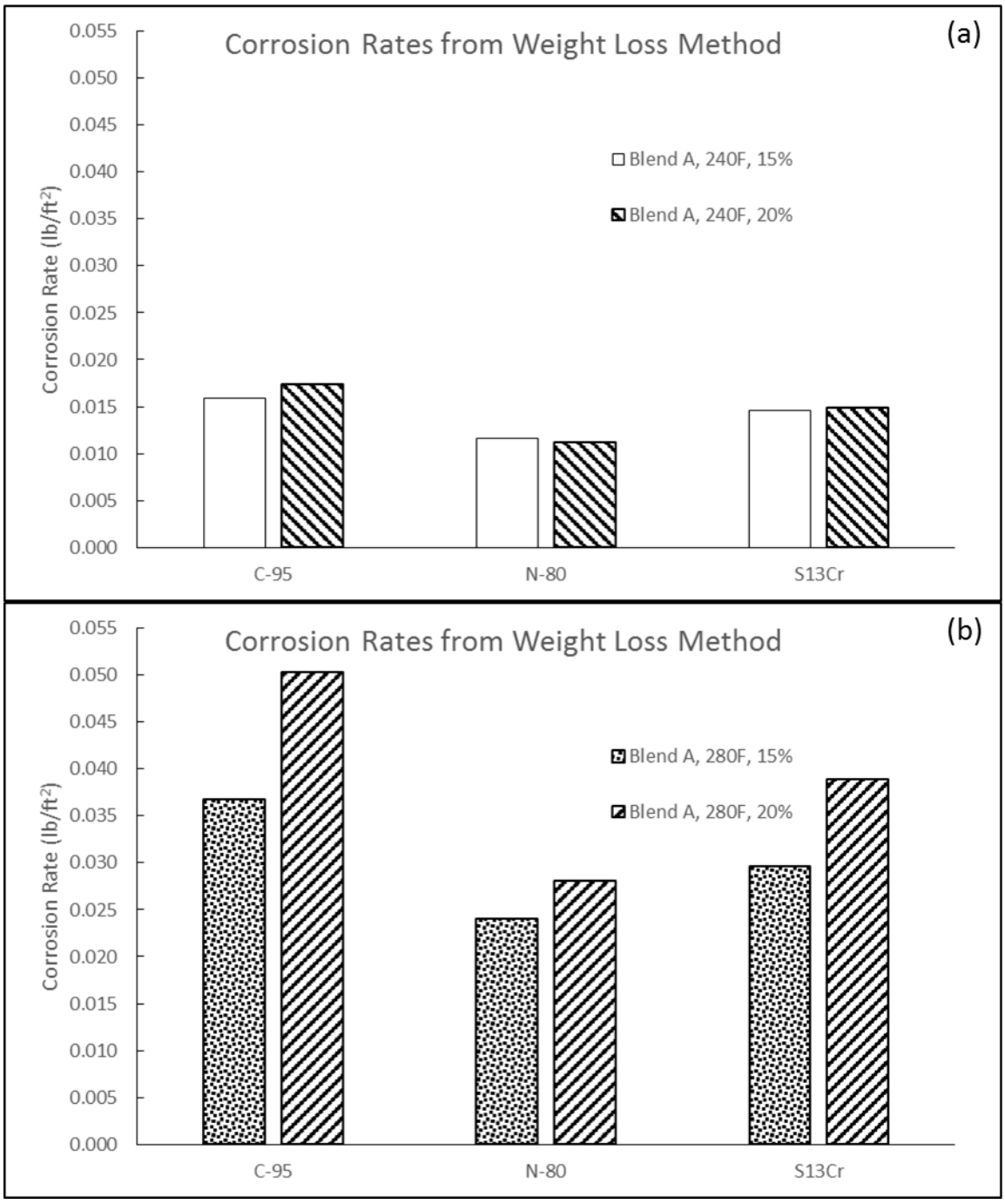

Figure 15: Corrosion rates at 15 wt% and 20 wt% acid at (a) 240°F and (b) 280°F.

For blend A, the corrosion rate of all three metals were observed to increase when the acid content was raised from 15% to 20% at 280°F compared to at 240°F despite a corresponding 1% increase in the amount of corrosion inhibitor as shown in Figure 15. This shows that as the temperature is increased, the effectiveness of inhibitor A decreases.

From the SDS provided for inhibitor A, thiourea polymer inhibitor base was found to be the active ingredient. Thiourea polymer inhibitor bases are formed by a reaction between formaldehyde, aromatic ketones, and thiourea, in the presence of a strong mineral acid, high temperature and a low molecular weight organic acid such as acetic acid (Cizek 2002). The final polymeric structure comprises of thiourea, the aromatic ketone, formaldehyde, and possibly the low molecular weight organic acid. As such, its inhibition capabilities must be due to the aromatic ketone, and thiourea.

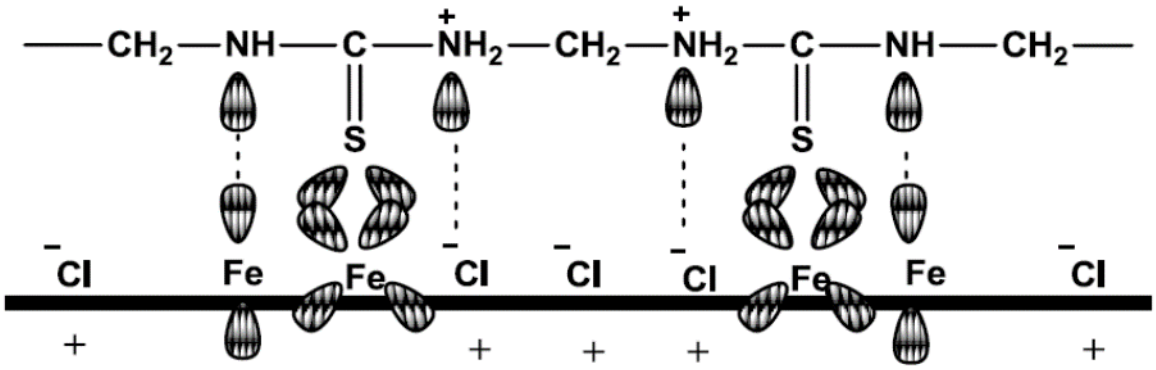

Figure 16: Bonding of thiourea-formaldehyde polymer to iron surface (Singh et al. 2014).

Thiourea adsorbs to the metal surface as shown in Figure 16. The sulfur group of thiourea and its derivatives attaches to the surface of the metal by donating its lone pair electrons to the vacant d-orbitals of Fe, Fe^{2+}, or Fe^{3+} on the surface (Loto et al., 2012). An increase in acid concentration results in the protonation of the thiourea molecule on its

sulfur and nitrogen groups. This results in a reduction of the inhibitory capability of the polymer because the hydrogen atom attached to the sulfur of thiourea will be brought in close to the metal surface through the interaction between the metal surface and the sulfur atom, allowing it to attack the surface with a lower activation energy (Pillai and Narayan 1979). Therefore the level of inhibition provided by thiourea is balanced between the concentration of protonated species and unprotonated ones.

Despite being a weaker base than sulfur, the nitrogen groups on thiourea derivatives can also be protonated in strong acids. Protonation of these groups reduces the charge density on the sulfur atom, thus weakening sulfur-metal interactions (Loto et al. 2012). Protonated nitrogen atoms can interact with already adsorbed Cl^- atoms through electrostatic attraction (physisorption) while unprotonated nitrogen atoms chemisorb to the metal surface using its lone pair (Singh et al., 2014). Similar to the sulfur atom, a higher acid concentration would result in increased protonation of the nitrogen groups resulting in a higher frequency of physisorption than chemisorption. Since chemisorbed thiourea derivatives provide higher inhibition, an increase in acid concentration would result in lowered inhibiting capabilities of the inhibitor (Loto et al., 2012).

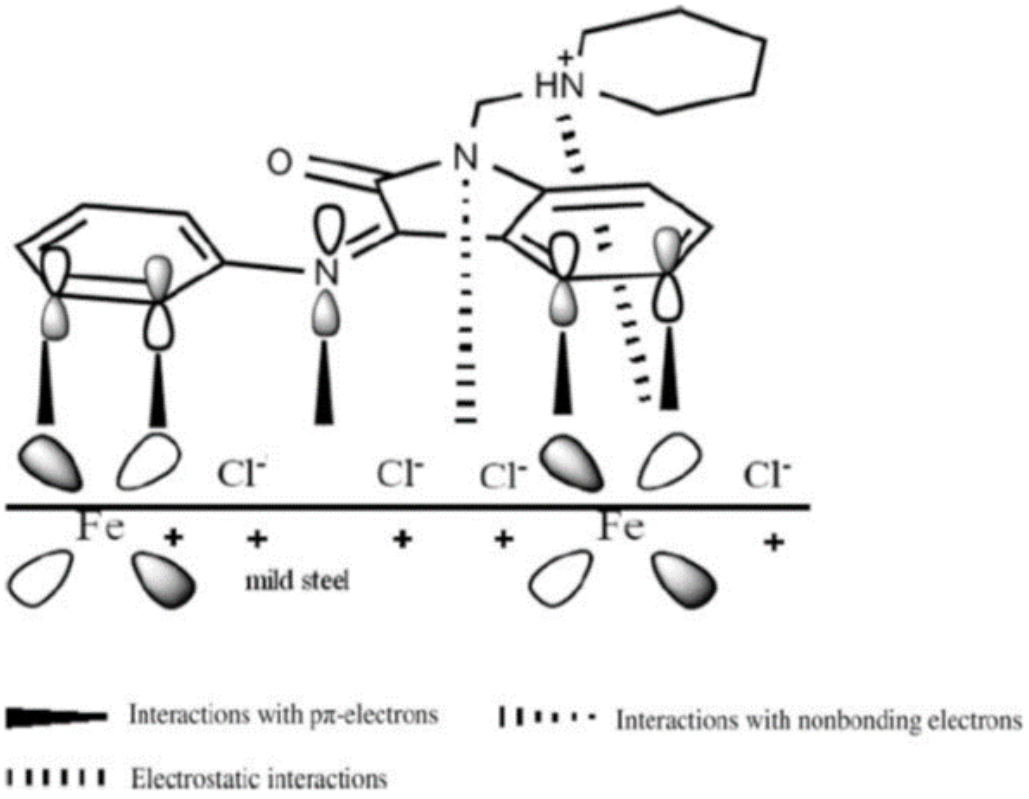

Figure 17: Adsorption of phenyl groups to steel surface (Ahamad et al. 2010).

The phenyl group in the polymer attaches itself to the metal surface through π bond interactions from the homocyclic ring and the vacant d orbitals of the metal surface (Ahamad et al., 2010). The phenyl group acts an anodic inhibitor due to the high electron density around the ring, reducing the anodic potential on the metal surface. However, since the phenyl group is neither a Lewis acid or base, its interaction with the metal surface should not influenced by acid concentration.

By knowing the interactions that determine the inhibitory capabilities of the active ingredient in inhibitor A, it can be determined that an increase in acid concentration would negatively impact the corrosion inhibiting capabilities of the polymer. Therefore,

additional inhibitor is required at higher acid concentrations and the addition of 1 vol% of inhibitor resulted in good protection of all 3 metals at 240°F as shown in Figure 15a. Increasing temperature further reduces the adsorption capability of thiourea to the surface of the metal thus despite adding more inhibitor, the corrosion rate still increased more significantly than at 240°F.

4.3 Reduction of blend B's effectiveness on N-80

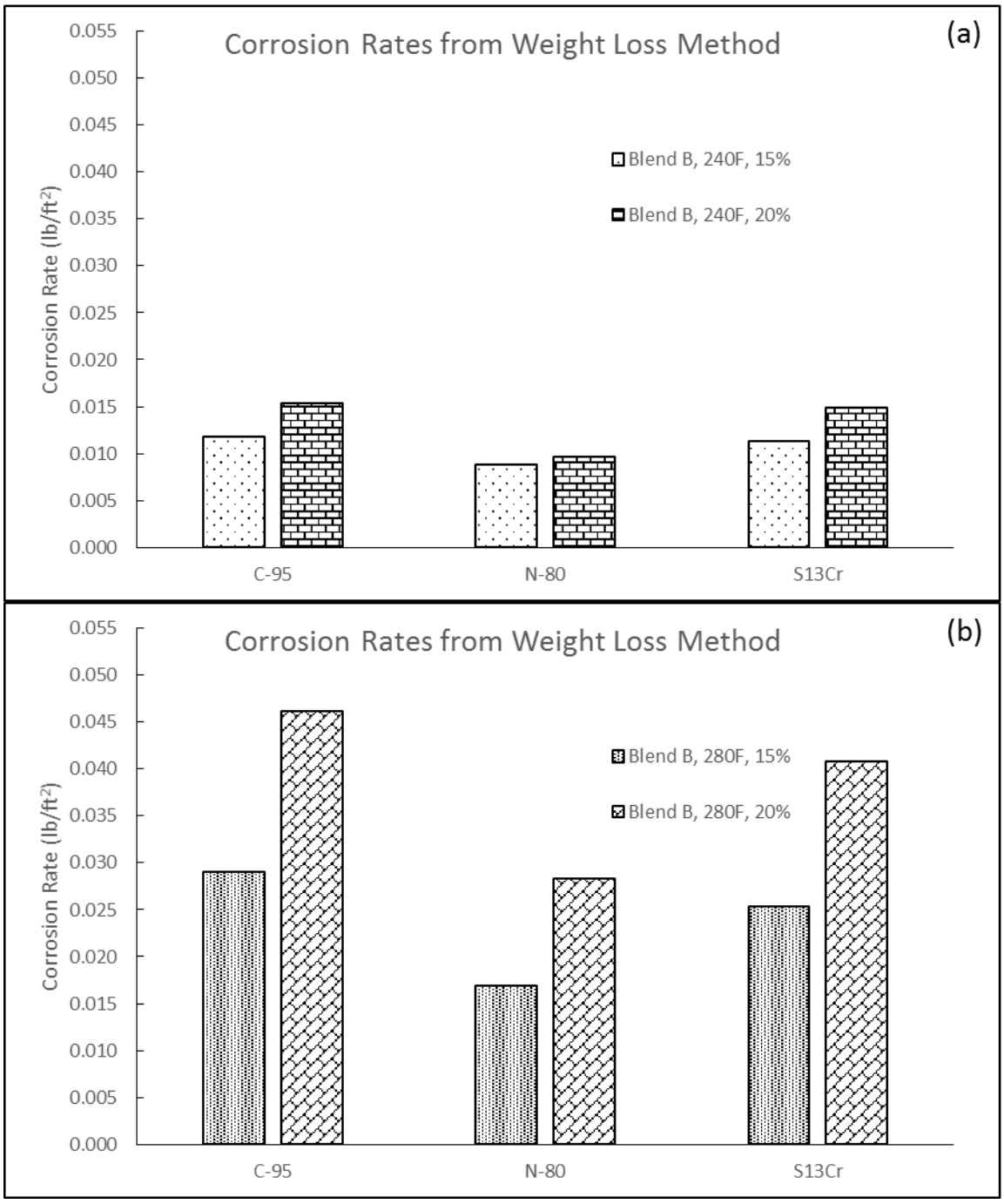

Figure 18: Corrosion rates of blend B for (a) 240°F and (b) 280°F.

At 240°F, blend B showed the best results with N-80 metal when the acid concentration was increased to 20% as shown in Figure 18. At this temperature, the increase in acid concentration showed increases in corrosion rates of C-95, N-80 and S13Cr of 29.9%, 9.2%, and 32.2% respectively. However, when the temperature was increased to 280°F, the effectiveness of inhibitor B appeared to decrease. The increase to 20% acid concentration resulted in an increase of 58.8%, 68.2%, and 61.4% for C-95, N-80 and S13Cr respectively.

This drastic reduction in protection of N-80 may be due competition between the inhibitor and formic acid to adsorb to the steel surface. The decomposition rate of formic acid increases with increasing temperature (Cassidy et al. 2007) which results in the formation of more iron carbide sites as described earlier. However, the presence of iron carbide has been shown to negatively affect the ability of corrosion inhibitors to protect the metal, with higher coverage of iron carbide resulting in greater reduction in the inhibiting capabilities of corrosion inhibitors (Xiong 2017). However, due to intellectual properties surrounding inhibitor B, further examination into the chemistry and reasons behind its interactions is not possible.

4.4 Viscoelastic Surfactants and Corrosion rate

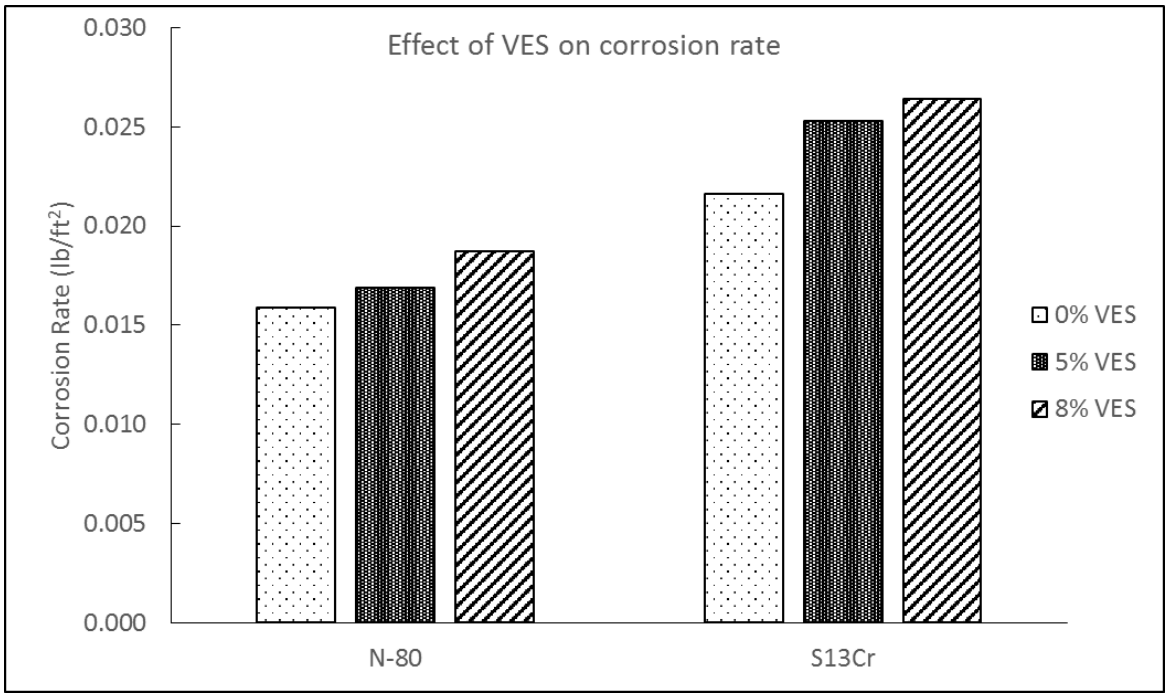

Figure 19: Effect of VES concentration on corrosion rate.

Figure 19 is a graphical representation of the data from Table 5 which shows the corrosion rates obtained for each test at different VES concentrations. As the concentration of VES was raised from 0% to 8%, the corrosion rate was observed to increase for both N-80 and S13Cr metals. The increments between VES concentration changes were mostly about 6% but that from 0 to 5% VES for S13Cr experienced a 17% increase in corrosion rate. These increments are likely due to competition between the VES and corrosion inhibitor for adsorption sites on the metal surface. Furthermore, the larger increase in corrosion rate of S13Cr than N-80 from 0 to 5% VES could indicate that the corrosion inhibitor intensifier plays a significant role at corrosion inhibition of N-80 than S13Cr.

This agrees with earlier observations that formic acid better protects N-80 than other metals.

While the type of corrosion inhibitor used in blend B cannot be determined, it is likely an organic corrosion inhibitor that contains a quaternary nitrogen group or is a sulfur-containing molecule since these groups of molecules are effective inhibitors for HCl (Frenier and Zaiuddin 2008). These organic corrosion inhibitors reduce corrosion rates by adsorbing to the surface of the metal through physisorption or chemisorption (Rostami and Nasr-El-Din 2009). VES molecules consist of a hydrophobic tail group and a hydrophilic head group which may be cationic, anionic, non-ionic but polar, or zwitterionic (Malik et al. 2011).

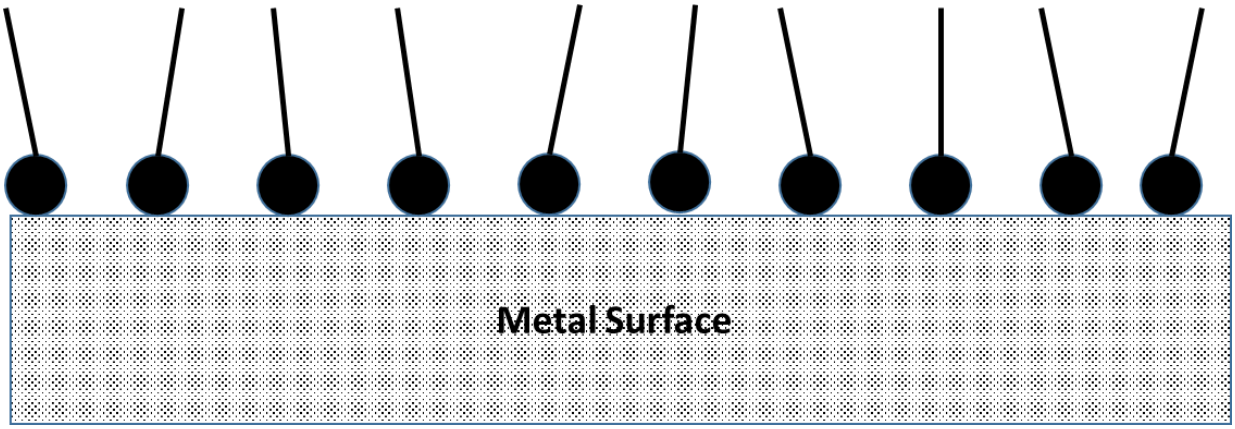

Figure 20: Schematic of surfactant adsorption to metal surface.

Surfactant molecules have previously been shown to act as and enhance the effects of corrosion inhibitors under various conditions (Free 2002; Fuchs-Godec and Pavlovic. 2012; Quej-Aké et al. 2015). Their ability to inhibit corrosion depends on their aggregating ability on the metal surface (Free 2002). Using their hydrophilic head, VES can adsorb to

the metal surface as shown in Figure 20 resulting in fewer available sites for the inhibitor molecule to adsorb to. Furthermore, electrostatic repulsion between the charged head groups and stearic effects between the hydrophobic tails of both the VES and inhibitor molecules may result in further difficulties for the corrosion inhibitor to adsorb to the surface. However, the extent of the change in corrosion rate should not be generalized to interactions between all VES and corrosion inhibitors. The chemistry of each molecule plays an important factor in determining the effect of VES on the inhibitory efficiency of the corrosion inhibitor and the corrosivity of each solution should be tested to determine this.

4.5 Green Coloration

As previously mentioned, pictures of the solution were taken to document any color changes before and after each test. The initial appearance of blend A solutions can be found in Figure 22 which can be described as a milky brown solution. When blend A was used with either of the carbon steel coupons, the end solution was observed to be brownish yellow in color. However, when it was used with S13Cr, the final solution was green instead.

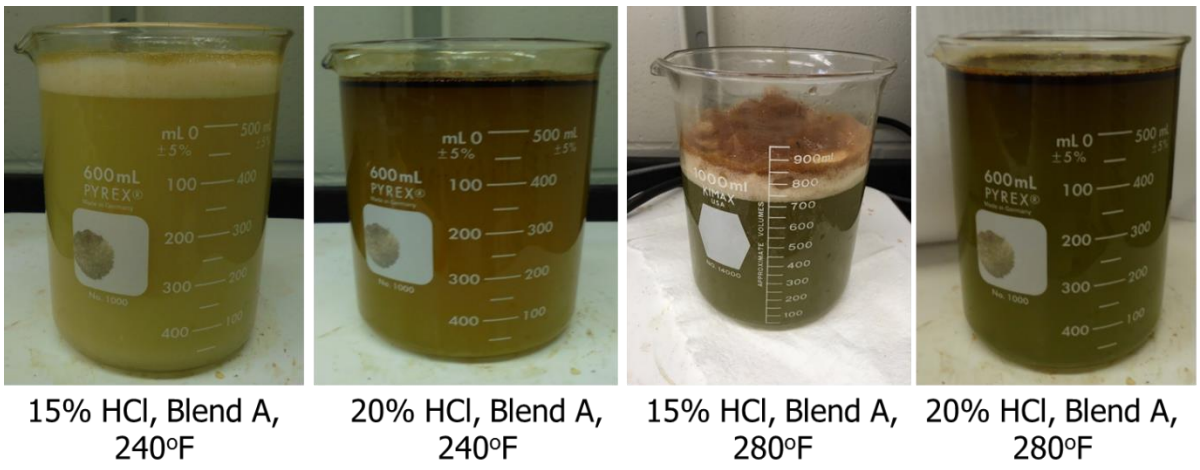

Figure 21: Green colored solutions after corrosion tests.

This is in contrast to blend B which yielded brown colored solutions in spite of whatever metal was tested as shown in Figure 23.

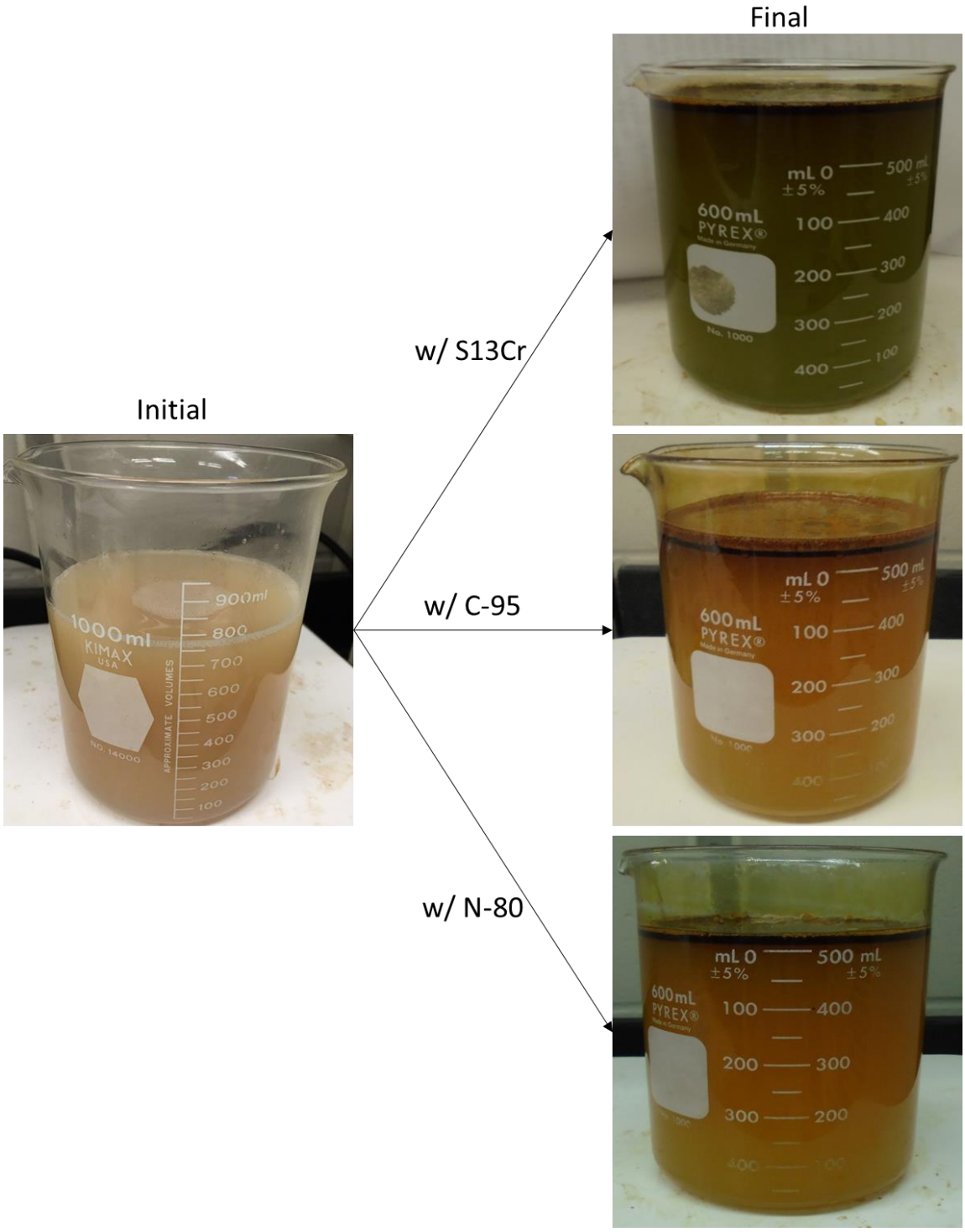

Figure 22: Example color change of blend A solution after each corrosion test. Green coloration observed when S13Cr is used.

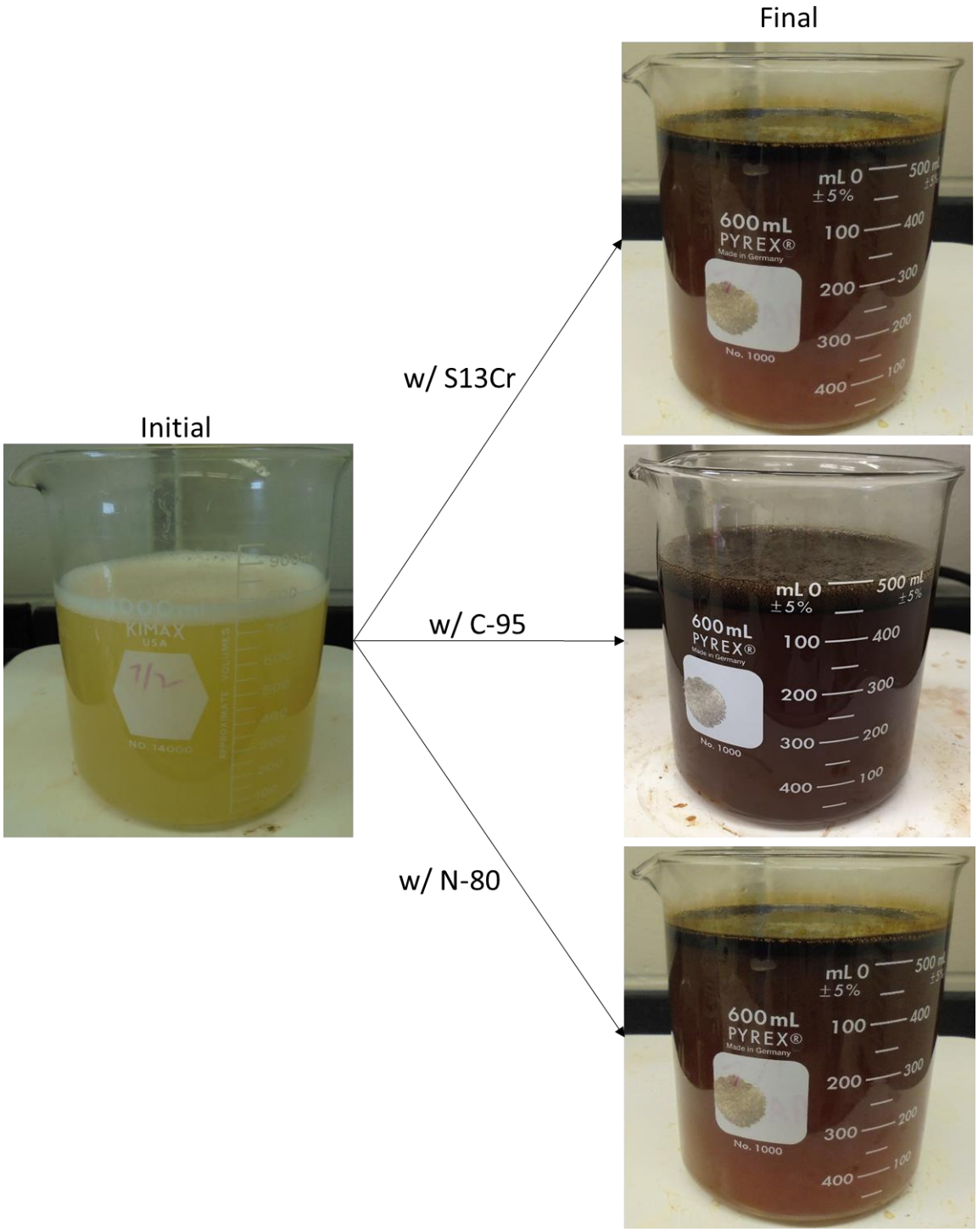

Figure 23: Example color change of blend B solution after each corrosion test. No differences in solution color were observed between metal types.

To determine the cause of the green coloration, ICP-OES was used to analyze the ion concentrations of iron, chromium, manganese, molybdenum, and nickel in each solution since all these ions are present in S13Cr. The results of blend A-S13Cr tests were then compared to blend A tests with carbon steel and to blend B tests.

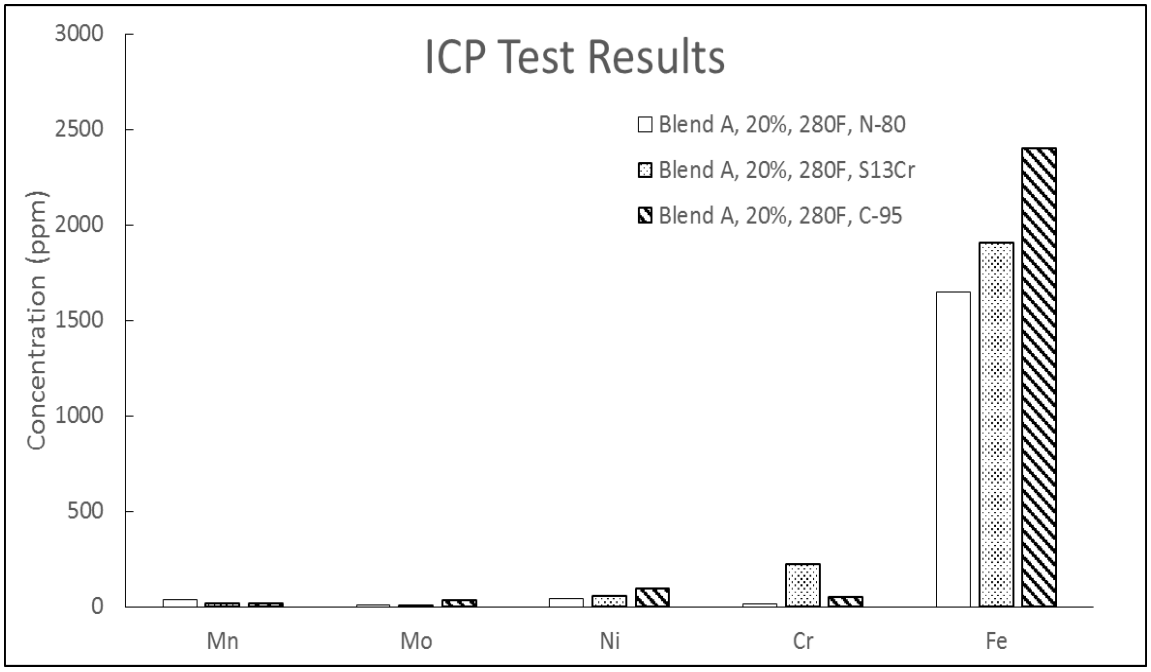

Figure 24: ICP-OES results for blend A tests at 20 wt% HCl with C-95, N-80, and S13Cr at 280°F.

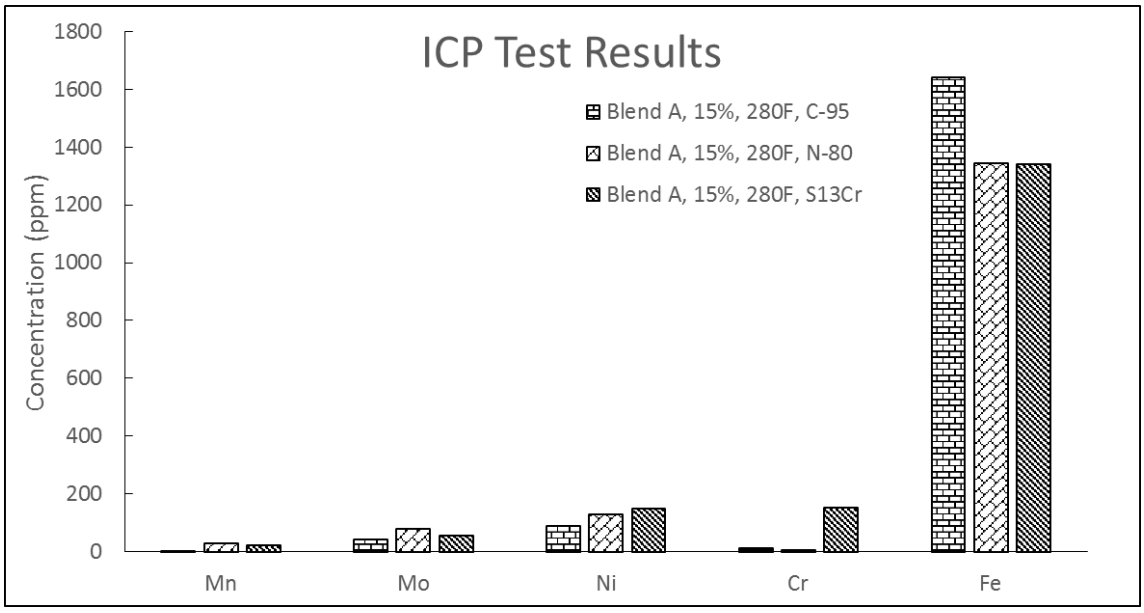

Figure 25: ICP-OES results for blend A tests at 15 wt% HCl with C-95, N-80, and S13Cr at 280°F.

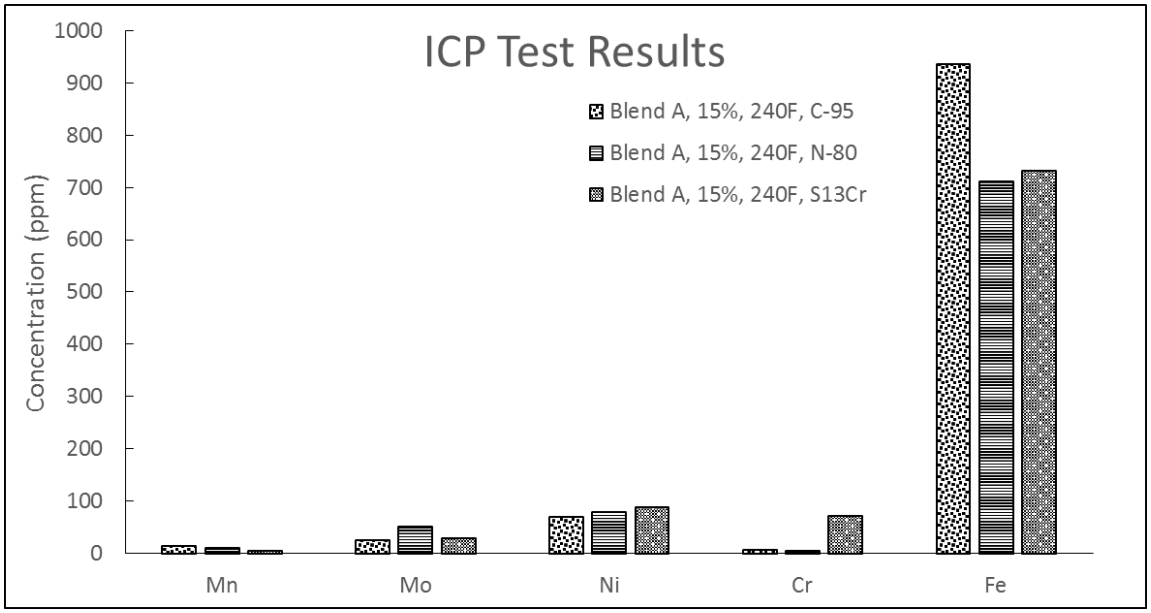

Figure 26: ICP-OES results for blend A tests at 15 wt% HCl with C-95, N-80, and S13Cr at 240°F.

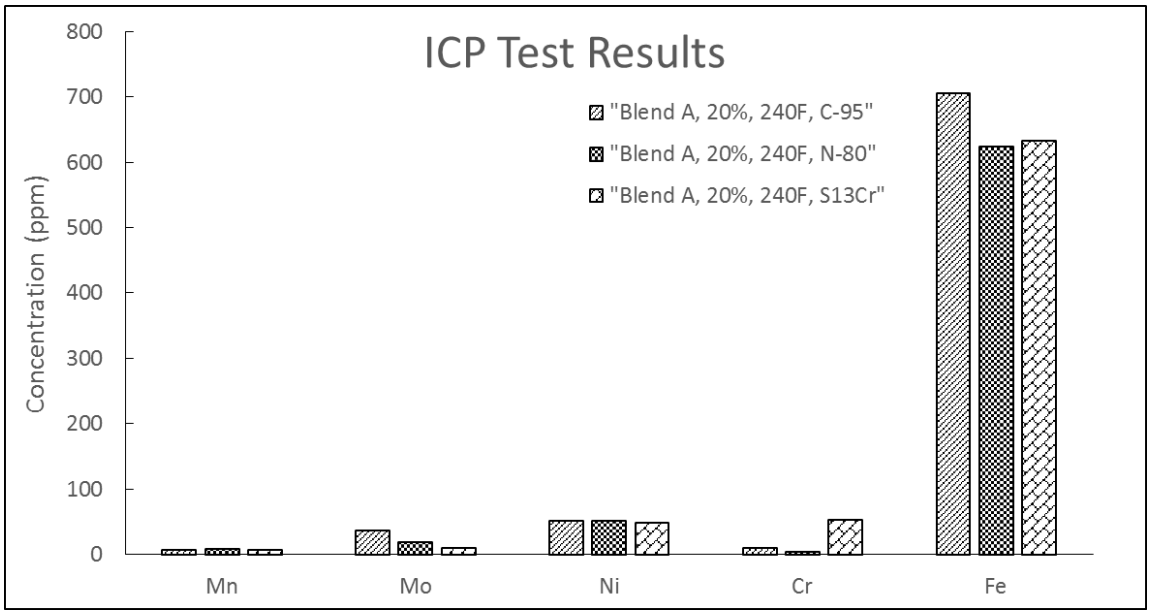

Figure 27: ICP-OES results for blend A tests at 20 wt% HCl with C-95, N-80, and S13Cr at 240°F.

Figure 24 to Figure 27 compares the ion concentrations of each metal type at each set of conditions. The main difference between the 2 carbon steels and S13Cr is the ion concentration of chromium and iron. The other ions are present in small quantities and are similar in concentration. However since the coloration of N-80 and C-95 solutions were the same, the green color must result from chromium (III) ions. To confirm this, filtered solutions of blend A – N-80 and blend A – S13Cr tests were prepared as shown in Figure 28 in order to establish a baseline color. The solutions obtained at 20 wt% and 280°F are used as an example since the color difference between them is the greatest. Also, N-80 solution was tested as the iron concentration was close to that of S13Cr, thus eliminating the possibility of iron being responsible for the difference in color.

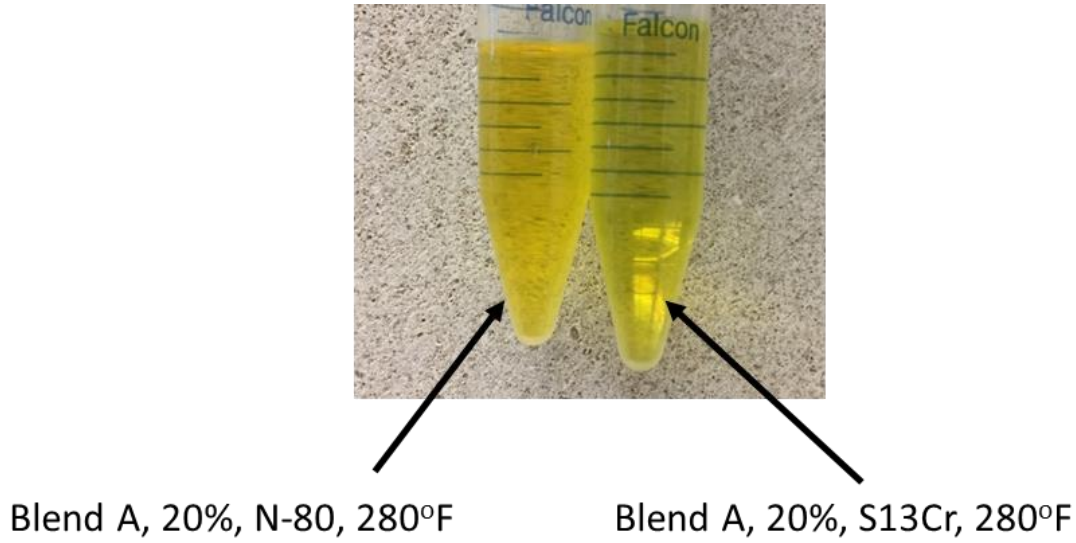

Figure 28: Filtered solutions of blend A-N-80 and blend A-S13Cr tests.

Crystals of $CrCl_3 \bullet 6H_2O$ were used to make a dilute solution containing 100 ppm $CrCl_3$. Drops of this solution were added to the filtered samples for blend A - N-80 tests and the resulting color compared to filtered solutions of blend A - S13Cr tests. The color comparisons are shown in Figure 29. From this comparison, it was deduced that Cr^{3+} was the cause of the green coloration.

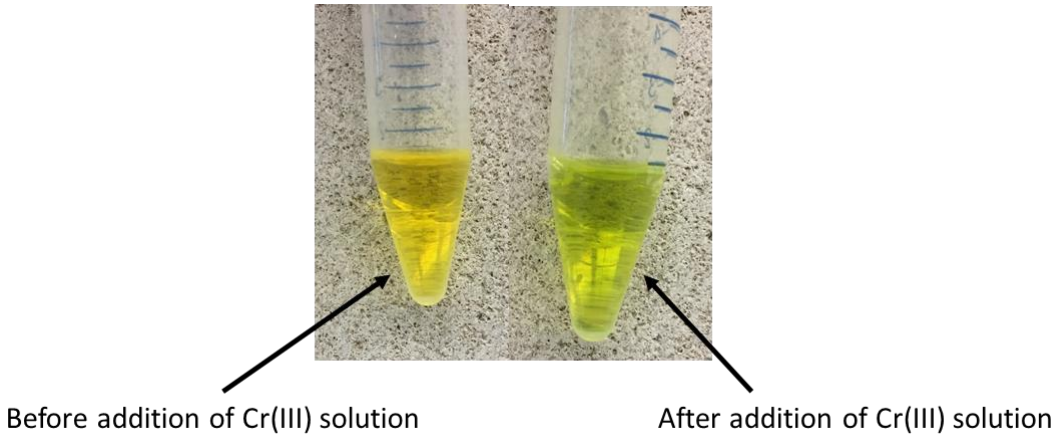

Figure 29: Addition of Cr^{3+} solution to blend A - N-80 solution. Change from yellowish brown to green color observed.

To understand the difference in coloration between blends A and B at the same conditions, the ion concentrations of blend B-S13Cr tests were compared to blend A. Using the same test conditions as in Figure 24, the ion concentrations were found to be similar for both solutions. The comparison can be found in Figure 30.

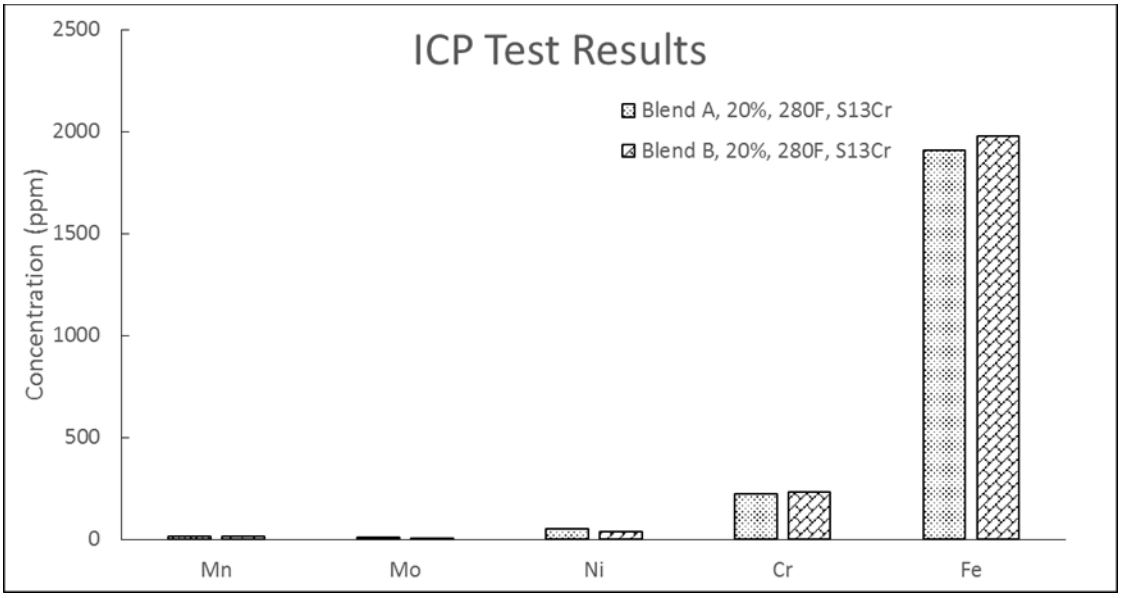

Figure 30: Comparison between ion concentrations of blends A and B for S13Cr with 20 wt% HCl at 280°F.

Similar observations can be made at all other conditions as shown in Figure 31 to Figure 33.

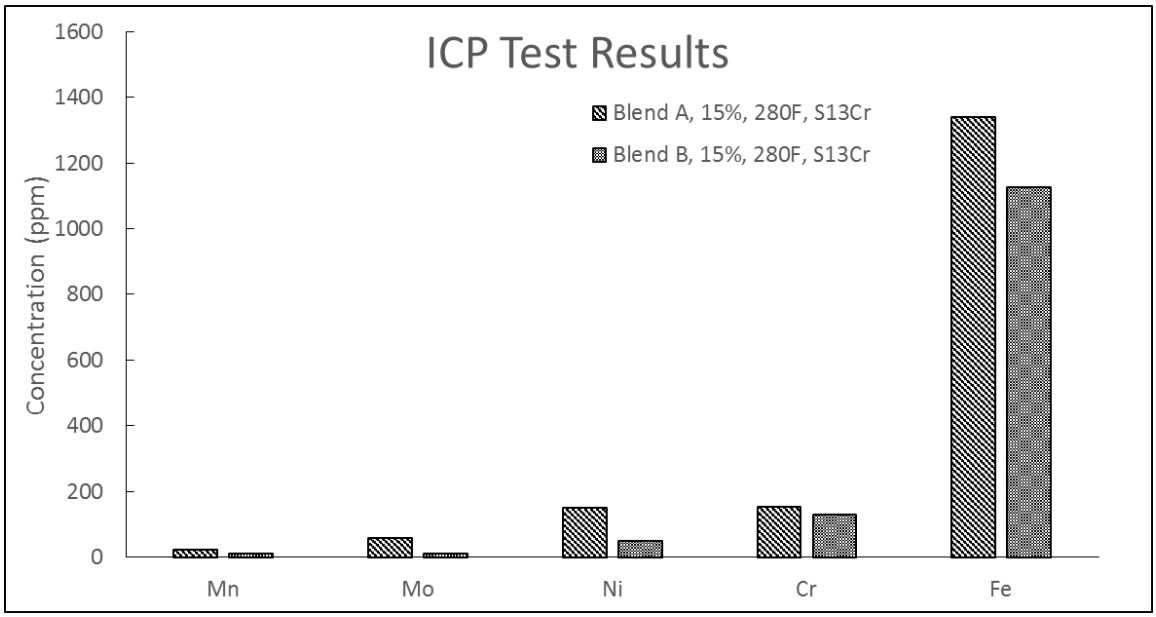

Figure 31: Comparison between ion concentrations of blends A and B for S13Cr with 15 wt% HCl at 280°F.

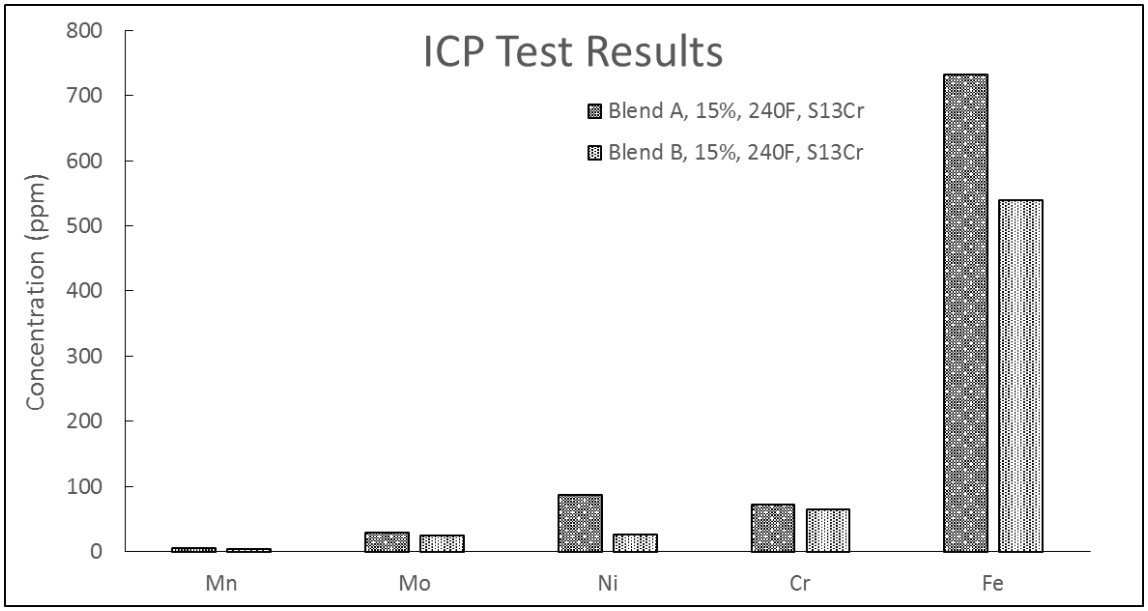

Figure 32: Comparison between ion concentrations of blends A and B for S13Cr with 15 wt% HCl at 240°F.

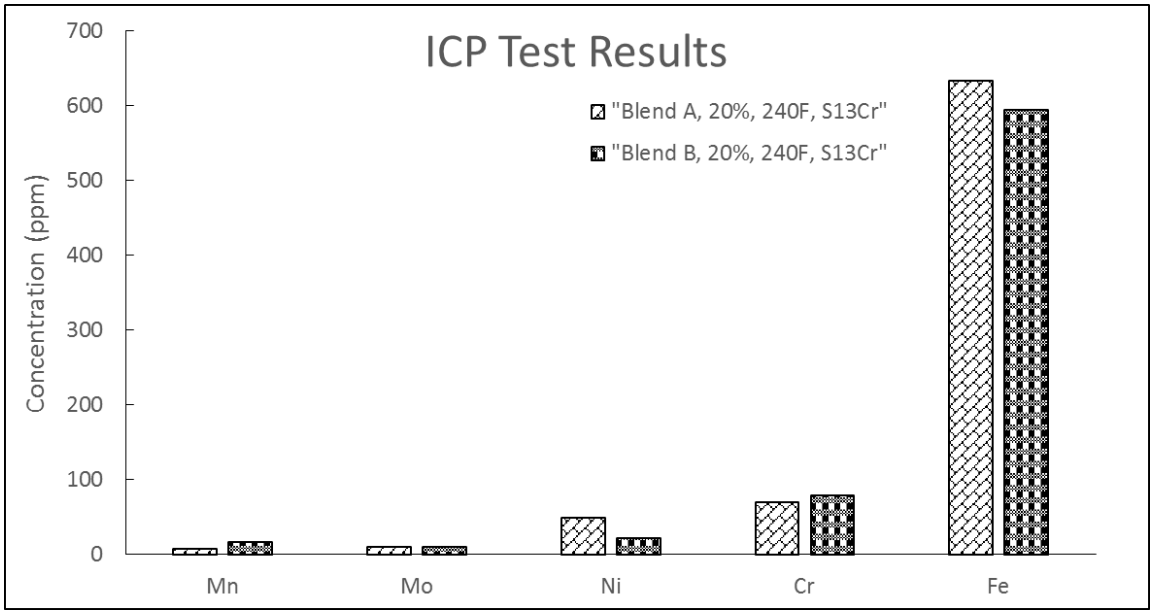

Figure 33: Comparison between ion concentrations of blends A and B for S13Cr with 20 wt% HCl at 240°F.

The lack of green color from blend B – S13Cr tests was likely to be a result of differences in the corrosion inhibitor used. Cervone et al. (1968) showed that thiourea and substituted thiourea have difficulties complexing with Cr^{3+} ions. The authors also observed a change in solution color from brown to green when Cr^{3+} - thiourea complexes underwent solvolysis. Therefore, the green coloration in blend A can be concluded to be a result of uncomplexed Cr^{3+} ions in solution. In blend B, it is likely that these ions were complexed by some molecule in the solution since a similar green coloration was not observed. Since iron control agents were present in both blends, it is unlikely that it was responsible for complexation of the Cr^{3+} ions.

5. FUTURE WORK

This work has identified several points of interest that could be further developed. This includes detailed studies of the interaction between N-80 steel and formic acid and the cause of the high levels of corrosion inhibition observed relative to other types of steel. Future work should also be done to understand the effect of VES and other surfactants on the inhibition efficiency of corrosion inhibitors. Since there are many different types of surfactants and corrosion inhibitors that are used in industry, a good understanding of their interactions may prove helpful in chemical selection when designing a new fluid blend.

6. CONCLUSIONS

In conclusion, both solutions tested display acceptable corrosion rates at 240°F but at 280°F and above, care must be exercised when applying these fluids. At higher temperatures, more corrosion inhibitor may be required or an alternate acidizing fluid should be used. Furthermore, from these tests, it was found that:

- N-80 metal had the lowest corrosion rate of all the tested metals. This is likely due to the interaction between the corrosion inhibitor intensifier and the metal surface to form some layer or intermediate that significantly inhibits H^+ attack.
- Blend A is a thiourea polymer based corrosion inhibitor that loses inhibition capability at higher acid concentrations and temperature due to the Lewis base properties of the inhibitor.
- The significant drop in inhibition efficiency on N-80 from 240°F to 280°F could be due to an unfavorable interaction between the inhibitor and the metal surface. However, the lack of information on the corrosion inhibitor prevents further analysis.
- Increasing the concentration of VES can negatively impact the corrosion on metal. This is due to competition between the VES and the organic corrosion inhibitor to bind to the surface of the metal.
- The green coloration of the solution was shown to be a result of free chromium (III) ions.

From this work, these 2 acid blends have been shown to meet industrial corrosion standards and can be applied in the field.

REFERENCES

Ahamad, I., Prasad, R., and Quraishi, M. A. 2010. Adsorption and inhibitive properties of some new Mannich bases of Isatin derivatives on corrosion of mild steel in acidic media. *Corrosion Science* **52** (4): 1472-1481. http://doi.org/10.1016/j.corsci.2010.01.015.

Al-Mutairi, S. H, Nasr-El-Din, H. A., Al-Muntasheri, G. A. et al. 2005. Corrosion Control During Acid Fracturing of deep Gas Wells: Lab Studies and Field cases. Presented at the SPE International Symposium on Oilfield Corrosion held in Aberdeen, UK, 13 May. SPE 94639.

API SPEC 5CT, Petroleum and natural gas industries—Steel pipes for use as casing or tubing for wells, eighth edition. 2005. Washington, D.C.: API.

Broden, G., Rhodin, T. N., and Brucker, C. 1976. Synchrotron radiation study of chemisorptive bonding of CO on transition metals — Polarization effect on Ir(100). *Surface Chemistry* **59** (2): 593-611. https://doi.org/10.1016/0039-6028(76)90038-8.

Bujise, M., de Boer, P. Breukel, B., et al. 2004. Organic Acids in Carbonate Acidizing. Presented at the SPE European Formation Damage Conference, The Hague, Netherlands, 13-14 May. SPE-82211-MS. https://doi.org/10.2118/82211-MS.

Cabello, G., Funkhouser, G. P., Cassidy, J. et al. 2013. CO and trans-cinnamaldehyde as corrosion inhibitors of I825, L80-13Cr and N80 alloys in concentrated HCl solutions at high pressure and temperature. *Electrochimica Acta* **97** (1): 1-9. http://doi.org/10.1016/j.electacta.2013.03.011.

Cassidy, J. M., McNeil, R. I. and Kiser, C. 2007. Understanding Formic Acid Decomposition as a Corrosion Inhibitor Intensifier in Strong Acid Environments. International Symposium on Oilfield Chemistry, 28 February-2 March, Houston, Texas, U.S.A. SPE-106185-MS. https://doi.org/10.2118/106185-MS.

Cervone, E., Cancellieri, P., and Furlani, C. 1968. Complexes of chromium(III) with thioureas. *Journal of Inorganic and Nuclear Chemistry* **30** (9): 2431-2436. https://doi.org/10.1016/0022-1902(68)80254-4.

Chang, F. F., Nasr-El-Din, H. A., Lindvig, T. 2008. Matrix Acidizing of Carbonate Reservoirs Using Organic Acids and Mixture of HCl and Organic Acids. Presented at the SPE Annual Technical Conference and Exhibition, Denver, Colorado, USA, 21-24 September. SPE-116601-MS. https://doi.org/10.2118/116601-MS.

Cizek, A. 2002. *Halogen Acid Corrosion Inhibitor Base*. International Patent WO2002103081 A2.

Craciunescu, C. and Hamdy A. S. 2013. The Effect of Copper Alloying Element on the Corrosion Characteristics of Ti-Ni and Ternary Ni-Ti-Cu Meltspun Shape Memory Alloy Ribbons in 0.9% NaCl Solution. *International Journal of Electochemical Science* **8** (2013): 10320-10334.

Craig, B. D. and Smith, L. 2001. *Corrosion Resistant Alloys (CRAs) in the oil and gas industry – selection guidelines update*, 3rd edition, North Carolina: Nickel Institute Technical Series.

Crowe, C. W., McGowan, G. R., and Baranet, S.E. 1988. Investigation of Retarded Acids Provides Better Understanding of Their Effectiveness and Potential Benefits. SPE Production Engineering 5 (2): 166-170. SPE-18222-PA. https://doi.org/10.2118/18222-PA.

Cunat, P. 2004. Alloying Elements in Stainless Steel and Other Chromium-Containing Alloys. *Euro Inox and International Chromium Development Association* **1**: 1-24.

Devereux, S. 1998. *Practical Well Planning and Drilling Manual*, first edition, Tulsa, Oklahoma: PennWell.

Ferhat, M., Benchettra, S., Amara, S., et al. 2014. Corrosion behaviour of Fe-C alloys in a sulfuric medium. *Journal of Materials and Environmental Science* **5** (4): 1059-1068.

Finsgar, M. 2014. Application of corrosion inhibitors for steels in acidic media for the oil and gas industry: A review. *Corrosion Science* **86** (2014): 17-41. http://dx.doi.org/10.1016/j.corsci.2014.04.044.

Fontana, M. G. and Greene, N. D. 1978. *Corrosion Engineering*, first edition, New York: McGraw Hill Education.

Free, M. L. 2002. Understanding the effect of surfactant aggregation on corrosion inhibition of mild steel in acidic medium. *Corrosion Science* **44** (12): 2865-2870. http://doi.org/10.1016/S0010-938X(02)00080-X.

Frenier, W. W. and Ziauddin, M. 2008. Formation, Removal and Inhibition of Inorganic Scale in the Oilfield Enviornment, first edition. Ricahrdson, Texas: Society of Petroleum Engineers.

Frenier, W. W., Hill, D. G. and Jasinski, R. J. 1989. Corrosion Inhibitors for Acid Jobs. Oilfield Review **1** (2): 15-21.

Fuchs-Godec, R. and Pavlovic, M. G. 2012. Synergistic effect between non-ionic surfactant and halide ions in the forms of inorganic or organic salts for the corrosion inhibition of stainless-steel X4Cr13 in sulphuric acid. *Corrosion Science* **58** (1): 192-201. http://doi.org/10.1016/j.corsci.2012.01.027.

Gaverick, L. 1994. Corrosion in the Petrochemical Industry, first edition, Ohio: ASM International.

Humpston, G. and Jacobson, D. M. 2004. *Principles of soldering*, first edition, Ohio : ASM International.

Jones, D. A. 1996. *Principles and Prevention of Corrosion*, 2nd edition, New Jersey: Prentice Hall.

Kalfayan, L. 2008. *Production Enhancement With Acid Stimulation*, p. 5. Tulsa: PennWell Corporation.

Kane, R. D. and Cayard, M. S. 1998. Roles of H2S in the Behavior of Engineering Alloys: A Review of Literature and Experience. Presented at the CORROSION 98, San Diego, California, 22-27 March.

Kehrer, V. J., and Leidheiser, H. 1954. The Catalytic Decomposition of Carbon Monoxide on Large Metallic Single Crystals. *Journal of Physical Chemistry* **58** (7): 550-555. http://dx.doi.org/10.1021/j150517a010.

Kodama, T. and Ambrose, J. R. 1976. Effect of Molybdate Ion on the Repassivation Kinetics of Iron in Solutions Containing Chloride Ions. *Corrosion* **33** (5): 155-161. http://dx.doi.org/10.5006/0010-9312-33.5.155.

Loto, R. T., Loto, C., and Popoola, P. 2012. Corrosion inhibition of thiourea and thiadiazole derivatives: A review. *Journal of Material Environmental Science* **3** (5): 885-894.

Ma, F. Y. 2012. Corrosive Effects of Chlorides on Metals. In *Pitting Corrosion*, ed. Bensalah, N. Chap. 7, 139-178. Intech.

Malik, M. A., Hashim, M. A., Nabi, F. et al. 2011. Anti-corrosion ability of surfactants: A review. *International Journal of Electrochemical Science* **6** (6): 1927-1948.

Nowack, B. 2002. Critical Review Environmental Chemistry of Aminopolycarboxylate Chelating Agents. *Environmental Science and Technology* **36** (19): 4009–4016. http://dx.doi.org/10.1021/es025683s.

Petersen, C. W. and Bleum, M. F. 1989. Requirements for Corrosion-Resistant Alloy (CRA) Production Tubing. Presented at the SPE Annual Technical Conference and Exhibition, San Antonio, Texas, 8-11 October. SPE-19727-MS. https://doi.org/10.2118/19727-MS.

Pillai, K. C. and Narayan, R. 1978. Inhibition of Corrosion of Iron in Acids by Thiourea and Derivatives. Journal of the Electrochemical Society 125 (9): 1393-1397. http://doi.org/10.1149/1.2131684.

Popoola L., Grema, A., Latinwo, G., et al. 2013. Corrosion problems during oil and gas production and its mitigation. *International Journal of Industrial Chemistry* **4** (1): 1-15. http://dx.doi.org/10.1186/2228-5547-4-35.

Quej-Aké, L., Contreras, A., Aburto, J. 2015. The effect of non-ionic surfactant on the corrosion inhibition of X52 pipeline steel in NaCl solutions. *International Journal of Electrochemical Science* **10** (2): 1809-1821.

Rostami, A., and Nasr-El-Din, H. A. 2009. Review and evaluation of corrosion inhibitors used in well stimulation. Presented at the SPE International Symposium on Oilfield Chemistry, The Woodlands. Texas, 20-22 April. SPE-121726-MS. http://dx.doi.org/10.2118/121726-MS.

Seth, K., Evans, B. A., and Gabrysch, A. D. 2011. Development and Testing of a Novel Corrosion Inhibitor Technology for Acid Corrosion. Presented at the SPE Middle East Oil and Gas Show and Conference, Manama, Bahrain, 25-28 September. SPE-142675-MS. https://doi.org/10.2118/142675-MS.

Singh, A. and Quraishi, M. A. 2015. Acidizing corrosion inhibitors: A review. *Journal of Materials and Environmental Science* **6** (1):224-235.

Singh, P., Quraishi, M. A., and Ebenso, E. 2014. Thiourea-Formaldehyde Polymer a New and Effective Corrosion Inhibitor for Mild Steel in Hydrochloric Acid Solution. *International Journal of Electrochemical Science* **9** (9): 4900-4912.

Tourky, A. R., Azim, A. A., and Anwar, M. M. 1965. Effect of carbon content on the corrosion and passivity of iron. *Corrosion Science* **5** (4): 301-317. https://doi.org/10.1016/S0010-938X(65)90636-0.

Townsend, H. E. 2001. Effects of Alloying Elements on the Corrosion of Steel in Industrial Atmospheres. *Corrosion Science* **57** (6): 497-501. http://dx.doi.org/10.5006/1.3290374.

Ueda, M., Amaya, H., Ogawa, K., et al. 1996. Corrosion Resistance of Weldable Super 13Cr Stainless Steel in H2S Containing CO2 Environments. Presented at the CORROSION 96, Denver, Colorado, 24-29 March.

Vaughn, G. A. and Greer \, J. B. 1980. High Strength Nickel-Alloy Tubulars For Deep, Sour Gas Well Application. Presented at the SPE Annual Technical Conference and Exhibition, Dallas, Texas, 21-24 September. SPE-9240-MS. https://doi.org/10.2118/9240-MS.

Xiong, Y. 2017. Impact of Pre-Corrosion on Corrosion Inhibitor Performance: Can We Protect Aged Pipelines? Presented at Corrosion 2017, New Orleans, Louisiana, 27-30 March.

Zhao, M. C., Tang, B., Shan, Y. Y., et al. 2003. Role of Microstructure on Sulfide Stress Cracking of Oil and Gas Pipeline Steels. *Metallurgical and Materials Transactions A* **34** (5): 1089-1096. https://doi.org/10.1007/s11661-003-0128-7.